# Design, Implementation, and Successful Test of a Prototype Hadron Blind Detector

A Thesis Presented

by

Robert P. Pisani

to

The Graduate School

in Partial Fulfillment of the Requirements

for the Degree of

Master of Science

in

Physics
(Scientific Instrumentation)

State University of New York
at
Stony Brook

December 1995

Copyright © by
Robert P. Pisani
1995

State University of New York
at Stony Brook

The Graduate School

Robert P. Pisani

We, the thesis committee for the above candidate for the Master of Science degree, hereby recommend acceptance of the thesis.

Thomas Hemmick
Project Director
Professor of Physics

Michael Marx
Professor of Physics

David Fossan
Professor of Physics

This thesis is accepted by the Graduate School.

Graduate School

# Abstract of the Thesis

# Design, Implementation, and Successful Test of a Prototype Hadron Blind Detector

by

Robert P. Pisani

Master of Science

in

Physics
(Scientific Instrumentation)

State University of New York at Stony Brook

1995

I have constructed and tested a threshold Čerenkov detector inspired by the conceptual design of Giomataris and Charpak[1]. The basic design consists of a gas radiator followed by a photosensitive wire chamber using a solid CsI photo-cathode. The photon detector lies directly in the particle path and is required to have single photo-electron sensitivity and yet be insensitive to the passage of a charged particle. We have altered the design by adding a thin (0.5 mm/$X_o$ = 0.3%) LiF window. This window allows one to separate the radiator and avalanche volumes, giving greater flexi-

bility in the gas choices. Our detector was operated with $C_2F_6$ as the radiator gas at lengths of 120, 80, and 40 cm. The avalanche gas was 95% $He$ + 5% $CH_4$. The detector was constructed at SUNY Stony Brook and was tested in the B2 Test Beam at the Alternating Gradient Synchrotron at Brookhaven National Laboratory. At 95% electron efficiency, the pion efficiency was 1/333, 1/150, and 1/100 for each of the lengths listed above.

This thesis is dedicated to Nancy.

# Contents

**List of Figures** . . . . . **xii**

**List of Tables** . . . . . **xiii**

**Acknowledgements** . . . . . **xiv**

**1 Introduction** . . . . . **1**

1.1 Background . . . . . 1

**2 Motivation and The Phenix Detector System** . . . . . **4**

2.1 Present Status . . . . . 4

2.2 HBD upgrade option . . . . . 6

2.3 Motivation . . . . . 7

**3 Principles of the HBD** . . . . . **10**

3.1 Čerenkov Radiation . . . . . 11

3.1.1 Definition . . . . . 11

3.1.2 Basic Physics of the Čerenkov Effect . . . . . 11

3.2 Photoelectric Effect . . . . . 13

3.3 Parallel Plate Avalanche Chamber . . . . . 14

3.3.1 The Avalanche . . . . . 14

3.4 Energy Loss and Ionization . . . . . 15

3.5 Radiation Length . . . . . 16

**4 Preliminary Work . . . . . 18**

4.1 Prototype Photo Detector Design . . . . . 18

4.1.1 Components and developed techniques . . . . . 20

4.1.2 Signal Feedthroughs . . . . . 21

4.2 CsI Deposition . . . . . 23

4.2.1 The Evaporation . . . . . 23

**5 Quantum Efficiency Of the Cathodes . . . . . 27**

5.1 Experimental Setup . . . . . 27

5.1.1 Pumping Station . . . . . 27

5.1.2 Flash Lamp . . . . . 28

5.1.3 Electronics . . . . . 31

5.1.4 Bench Triggering . . . . . 31

5.2 Measurements . . . . . 32

**6 Additional Bench Tests . . . . . 35**

6.1 Avalanche Gas Mixture . . . . . 35

6.2 Radiator gas . . . . . 38

6.3 PPAC Conditions . . . . . 39

**7 Hadron Blind Detector Design** . . . . . **40**

7.1 Radiator Vessel . . . . . 40

7.2 Gas Flow . . . . . 44

7.3 Support Equipment for Radiator Vessel . . . . . 44

7.4 Transparency Monitor . . . . . 46

7.5 Photon Detector . . . . . 47

7.5.1 LiF Window Support . . . . . 48

7.5.2 Upper Lid . . . . . 51

7.5.3 Anode Mesh . . . . . 52

7.5.4 Grid Spacer . . . . . 52

7.5.5 Lower Lid . . . . . 53

7.5.6 Pad Plane . . . . . 53

7.5.7 PPAC and CsI supporting material . . . . . 56

7.5.8 Back Flange . . . . . 58

7.6 PPAC Region . . . . . 60

7.7 Evaporation and Assembly . . . . . 62

7.8 Fabrication Issues . . . . . 64

7.9 Electronics . . . . . 69

7.9.1 Preamplifier . . . . . 71

7.9.2 Shapers . . . . . 71

**8 Beam Tests** . . . . . **72**

8.1 Run History . . . . . 72

8.2 Trigger and Hit Definition . . . . . 74

8.3 Data Analysis . . . . . 79

8.3.1 The 120 Centimeter Length . . . . . 79

8.3.2 The 80 and 40 Centimeter Lengths . . . . . 92

**9 Conclusion** . . . . . **94**

# List of Figures


2.1 PHENIX Detector System . . . . . 5

2.2 Charpak's proposed HBD . . . . . 7

2.3 Stony Brook's proposed HBD . . . . . 8

3.1 Čerenkov shock wave . . . . . 12

3.2 Sketch of avalanche . . . . . 14

4.1 Small prototype detector . . . . . 19

4.2 Custom feedthroughs . . . . . 22

4.3 Schematic of evaporator . . . . . 25

5.1 Light source setup . . . . . 29

5.2 Schematic of electronics to PPAC . . . . . 30

5.3 Diagram of bench trigger . . . . . 32

6.1 Absorption curves for hydrocarbons . . . . . 36

7.1 Hadron Blind Detector Diagram . . . . . 41

7.2 Back flange and Detector Housing . . . . . 42

7.3 Hadron Blind Detector Photo . . . . . 43

7.4 Gas flow for the HBD . . . . . 45
7.5 Radiator vessel support equipment . . . . . 47
7.6 Photon detector expanded view . . . . . 49
7.7 Detector Parts . . . . . 51
7.8 Photo of lower Lid . . . . . 54
7.9 Sketch of pad Plane . . . . . 55
7.10 Photo of partially assembled photon detector . . . . . 57
7.11 Photo of photon detector mounted to back flange . . . . . 59
7.12 Sketch of the assembled PPAC region . . . . . 61
7.13 Photo of photon detector in evaporator . . . . . 63
7.14 Front and back side of detector plane . . . . . 65
7.15 Schematic of HBD electronics. . . . . 70

8.1 Configuration of the external triggers at the B2 test beam . . 75
8.2 Triggers electronics at the B2 test beam . . . . . 76
8.3 Sample plots of trigger signals . . . . . 77
8.4 Photo of electronics setup . . . . . 78
8.5 Signal from anode signal . . . . . 80
8.6 Single channel histogram . . . . . 81
8.7 25 pion events . . . . . 82
8.8 25 electron events . . . . . 83
8.9 Mean number of pads hit . . . . . 84
8.10 Distribution of hit pads and total charge for 1.2m . . . . . 86
8.11 Total charge plotted verse the number of pads that fire for 1.2m 87

8.12 HBD's efficiency at 1.2m . . . . . 88

8.13 e/pi separation for 80 and 40 cm . . . . . 89

8.14 HBD's efficiency at 80cm . . . . . 90

8.15 HBD's efficiency at 40cm . . . . . 91

# List of Tables

7.1 Radiation lengths . . . . . 68

8.1 Detector Efficiency . . . . . 92

# Acknowledgements

I would like to first thank Nancy. Without your constant support and encouragement, I could not have made it. Thank you for everything.

I would like to thank Dr. Tom Hemmick. He was more than just an advisor; he was a friend. I especially would like to thank him for his expertise which he shared during the project and also for his eagerness to stay awake for many days on end during the "crunch" time. Thanks for the many stories that made the time pass less dreadfully.

A special thanks goes to Tim Piazza, Steve Johnson and Thongbay Vongpaseuth for dropping everything else during the test beam run to give a hand. Thanks also to Sergey Panitkin who help set up our computer both at Stony Brook and at Brookhaven. I would also like to thank Rich Hutter for his help and advise during the projects duration.

Thanks to Craig Woody and the 877 collaboration for the loan of equipment during the projects duration. The detector would have never been completed without it. I am also grateful to David Anderson of the Particle Detector Group at Fermi National Laboratory. I would like to thank him for supplying the mesh and the CsI crystals and especially for the advice during the evap-

oration. I would also like to thank Mike Akopyan, a postdoc from MIT, for coming down to Stony Brook to lend a hand during our test run.

I want to thank the Dr. Peter Paul, Rich Lefferts and A.R. Lipski of Nuclear Structure Group for freely lending me equipment, lab space and especially for the use of the thermal evaporator.

I thank Brant Johnson for juggling the test beam schedule after our low purity bottle of $CF_4$ was discovered. All data at 80 cm and 40 cm lengths were taken during time he found "in the margin". I also thank Dave Dayton, Alan Carroll, and everyone in the AGS crew for their assistance during our run.

I want to thank all my friends. A special thanks goes through Chuck Jordan a fellow MSI student. I was great going through it together. Thanks for all the help and for listening to and helping with problems as they occured.

I would also like to thank Mr. B. Dawkins for his sharing of his expertise and especially for finding the solder and flux for the soldering of the stainless steel mesh.

Finally, I must acknowledge my family, my parents, my brother and sister, for their love and support, and for always reminding me that the hard work would pay off. Thank you.

# Chapter 1

# Introduction

In this thesis, the design, construction and test results of a working Hadron Blind Detector (HBD) are described in detail.

## 1.1 Background

Nuclear and high energy experiments are evolving towards the production of very high particle densities. As a result of this, particle detection, selection, and identification directly in the trigger has become increasingly critical.

A Čerenkov detector operated in threshold mode is the textbook example of a species dependent detector. However, Čerenkov detectors are difficult to implement in a compact layered or hermetic detector due to the need for focusing optics (which often create dead detector space), long radiator lengths, and thickness (in radiation lengths) of the photo-sensitive layer.

During the past several years the new solid CsI photocathode wire chamber techniques have shown increasing promise[2, 3, 4, 5, 6]. Rings have been

successfully observed in mirror focusing[7] and proximity focusing[8, 9, 10] configurations. Additionally, the initially disparate reports on quantum efficiency (QE)[11, 12, 13] have somewhat converged[14, 15, 9, 16] as photocathode production techniques[17, 2, 18] and quantum efficiency measurement standards have been improved[19].

An especially interesting configuration of a CsI photocathode Čerenkov detector was suggested by Giomataris and Charpak in 1991[1]. A sketch of this design is shown in Figure 2.2. Charged particles pass through the radiator gas. Čerenkov photons created by particles above threshold (v > c/n) pass through the anode mesh and are intercepted by the cathode. Photoelectrons created at the cathode avalanche toward the anode in a Parallel Plate Avalanche Chamber (PPAC) gap. This "windowless" configuration maximizes the photo-electron yield since the low wavelength cutoff is set by the transmission properties of the gas, not by a window. When run in threshold mode, the detector can be set to be sensitive to electrons and insensitive to pions and higher mass particles and has thus been dubbed a Hadron Blind Detector or HBD.

The requirements on the HBD radiator gas are numerous. The gas must simultaneously provide a high index of refraction, excellent transparency, good avalanche characteristics, and chemical compatibility with the photocathode. An experiment using pure $CF_4$ as the operating gas met with only limited success[20]. Although $CF_4$ gas does provide a high index of refraction ($n$= 1.0006) and excellent transparency (down to 106 nm), it is highly electronegative. It is presently suspected that the relatively small electron signal

found by that experiment was the result of absorption of photo-electrons prior to avalanche, frequently and effectively eliminating the signal. Additionally, there could be detrimental chemical interactions between the CsI layer and free $F^-$ ions created during avalanche[14], making $CF_4$ a less than optimal avalanche gas choice.

We have altered the HBD design to include a very thin LiF window to separate the radiator from the avalanche gas shown in Figure 2.3. At 0.5 mm thickness, the window accounts for very little material (.5mm/$X_o$= 0.3%)[1] and thereby does not violate the requirement that the detector be low mass. Additionally, the cutoff wavelength of LiF is near 120 nm and so it does not limit the sensitive wavelength range. We have constructed and tested an HBD using this design principle as a prototype detector for the PHENIX experiment[21] (one of four experiments presently under construction at the Relativistic Heavy Ion Collider (RHIC) accelerator at Brookhaven National Laboratory). I describe here the design, construction, and successful testing of our prototype.

[1]Here $X_o$ is the radiation length of the material and is defined as being the mean distance over which a high-energy electron loses all but $1/e$ of its energy by bremsstrahlung.

# Chapter 2

# Motivation and The Phenix Detector System

The Hadron Blind Detector is sought after as an upgrade to the PHENIX Detector System. In this chapter, I will briefly descuss the upgrade option for the Hadron Blind Detector (HBD) and the motivation behind its design and construction.

## 2.1 Present Status

Figure 2.1 shows the detector system as it is presently conceived. The goal of the PHENIX collaboration is to measure as many potential signatures of the guark-gluon plasma (QGP) as possible to determine if any of the physics variables show a simultaneous anomaly due to the formation of QGP [21]. The core measurement is the di-electron mass spectrum near midrapidity. In addition to its present "day-one" subsystems shown in the Figure 2.1, The PHENIX detector has several upgrade options. One of which is a Hadron Blind Detector.

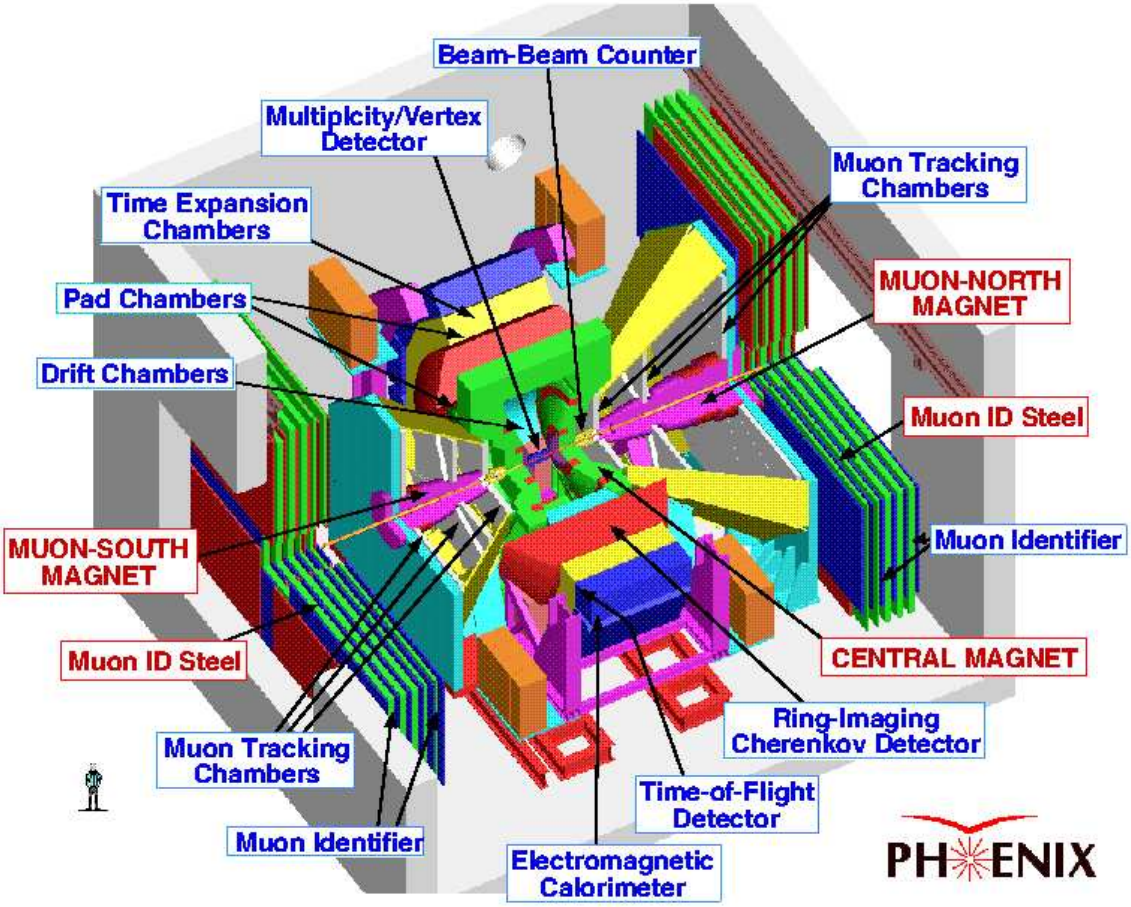


Figure 2.1: This is the PHENIX detector system as presently planed.

## 2.2 HBD upgrade option

One upgrade option considered PHENIX is the insertion of a Hadron Blind Detector near the collision point. A second magnet coil would be inserted into the system to cancel the magnetic field over the first 80 cm. Therefore, the HBD must be designed to operate within a 40 cm distance.

The HBD has three main functions. Its primary job is to act as a Dalitz rejector. In a centeral collision at the Relitivistic Heavy Ion Collider at BNL, roughly 10,000–20,000 particles will be produced. A many of these will be $\pi^o$. 1.2% of these pions will decay into a photon and a virtual photon. This virtual photon will decay to a $e^+$ and $e^-$ pair. This pair of electrons is a Dalitz pair($\pi^o \rightarrow \gamma\gamma^* \rightarrow \gamma e^+ e^-$).

It second function is to provide additional separation of electrons from hadrons. Finally, it may be possible to use the HBD as an on-line electron trigger in low multiplicity collisions.

With these functions in mind, the requirements for the HBD emerge.

- Needs to be compact (fit in radius of 40cm)
- Large area, stable PPAC running at 1 ATM
- High efficiency for Cherenkoc radiation
- Fast Single photon response
- Minimal dead region
- Minimal material of detector itself.

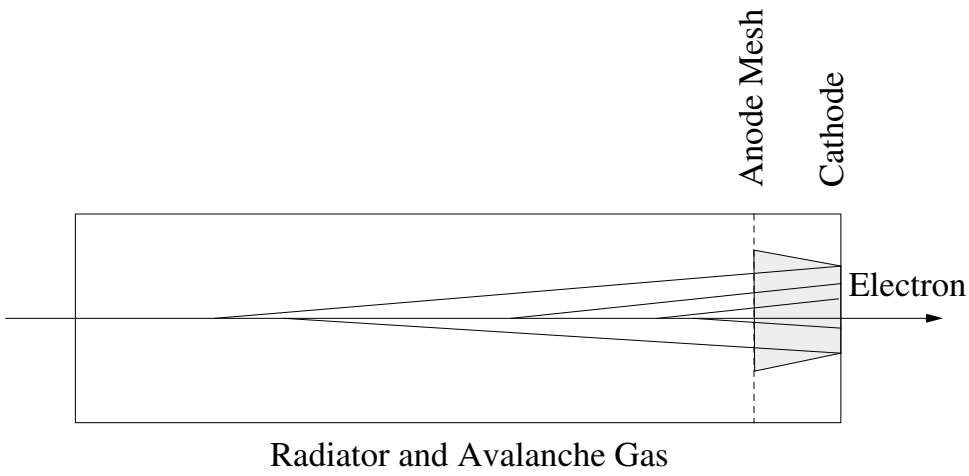


Figure 2.2: Charpak's proposed HBD. The same gas would be used for both the radiator and avalanche regions.

## 2.3 Motivation

The first HBD was proposed by Giomataris and Charpak[39]. Their detector was an in-line Čerencov detector in which the particles would travel through the photon detector. The prescription was to use a $He + .3\% CF_4$ mixture as the avalanche gas. This conceptual design called for the used of the same gas for the radiator and the avalanche. This gas mixture had a very small $dE/dx$ and a wavelength cut off at about 106nm. Because of its low index of refraction, however, too few photons would be produced at 40cm. A skematic of their detector concept is shown in figure 2.2.

Min Chen, et. al., of MIT constructed a prototype HBD using $CF_4$ as both the radiator and avalanche gas. This gas has a high index of refraction

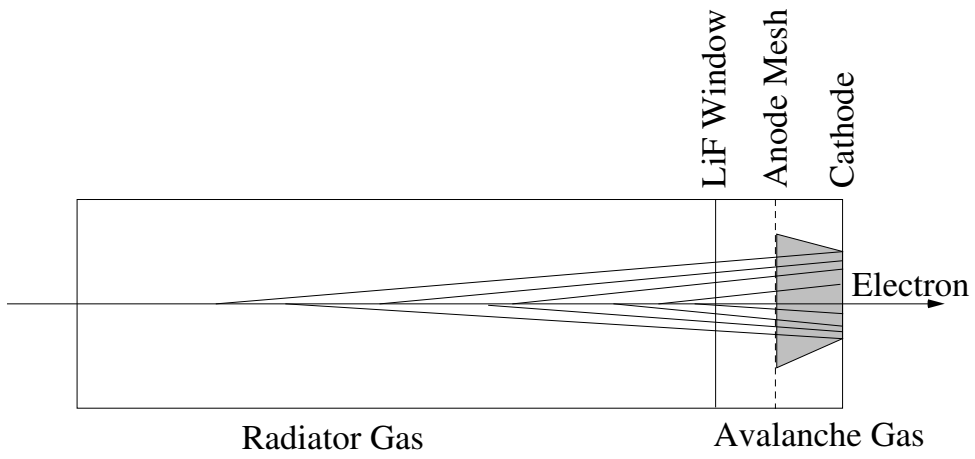


Figure 2.3: Stony Brook's proposed HBD. By adding the LiF window into the design. The radiator and avalanche regions are separated. This allows the used of different mixtures in each section.

---

(n=1.0006) and a low wavelength cutoff (106nm). This gas should produce many Čerenkov photon. That group found, however, that this gas steals electrons produces in the avalanche region which thereby reduces the signal. $CF_4$ is also an etching gas and when put into a high electric field as in an avalanche region, many $F^-$ are made which can eat away the materials of the anode and cathode.

In September 1994, SUNY Stony Brook was selected to take over the HBD research and development effort. It was decided that the Stony Brook HBD would have separate radiator and avalanche regions. The original plan was to use $CF_4$ as the radiator gas and $He + .3\% CF_4$ as the avalanche gas

with a .5mm LiF window between them. This was later change to $C_2F_6$ and $He + 5\% CH_4$ after bench tests of the original gas mixtures failed. Figure 2.3 shows the addition of the window to Charpak's original design.

# Chapter 3

# Principles of the HBD

There are several ways to detect a charged particle. One way is to detect the charge produced by particle as it losses energy during its travels through matter. Another method is to detect the Čerenkov light produced by a fast charged particle as it travels through material. For the case of an HBD, one should minimize the energy loss signal (common to all charged particles) and maximize the čerenkov signal. Our solution to this seeming impossibility was to choose different gases for the radiator and detector avalanche.

The transverse momentum spectrum of particles leaving the collision zone falls exponentially with increasing transverse momentum and is quite similar across all produced particle species. The electron is two orders of magnitude lower momentum than the next highest produced particle. Thus a Čerenkov detector with a judiciously chosen index of refraction can be mode sensitive to nearly all produced electrons while being insensitive to nearly all other particles.

Once a Čerenkov photon is produced, it must be detected. Some exper-

iments use photomultiplier tubes (PMT's) to do this. The draw back to this technique is that PMT's are expensive, provide only limited active area, and would be impossible to use in the path of a particle. Because of these considerations, UV sensitive parallel plate avalanche chambers were developed to detect the photons[29].

## 3.1 Čerenkov Radiation

### 3.1.1 Definition

Čerenkov radiation is an electro-magnetic shock wave that is produced when a charged particle travels through a dielectric medium with a velocity, $v$, greater than the velocity of light in that medium ($c/n$). The light is created at a fixed angle with respect to the direction of the particles travel.

### 3.1.2 Basic Physics of the Čerenkov Effect

Čerenkov radiation appears as a continuous spectrum of frequencies. The threshold for Čerenkov light production is dependent on the index of refraction,$n$, of the dielectric medium through which the particle travels. This threshold is set by the following condition [26]:

$$\beta \geq \frac{1}{n} \tag{3.1}$$

where $\beta$ equals $v/c$. This Čerenkov light emerges as a conical wavefront which is formed at an angle, $\theta$, with respect to the trajectory of the particle, such

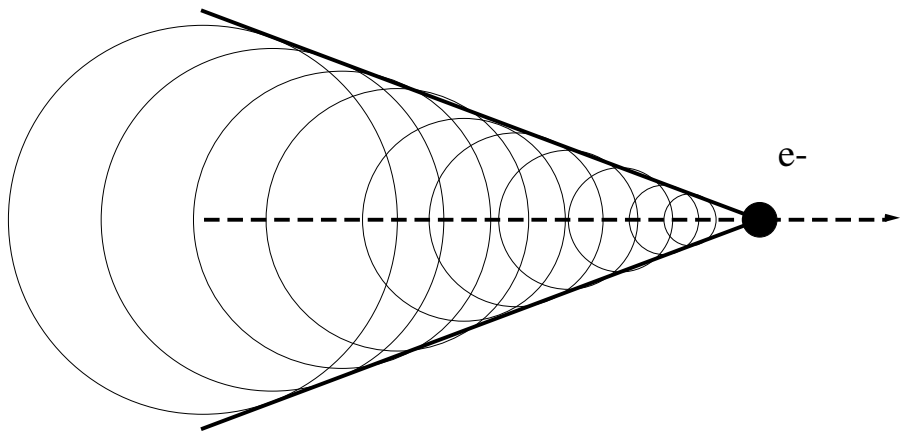


Figure 3.1: Formation of the Čerenkov shock wave as a particles travels through a medium with sufficient energy.

---

that [24]:

$$cos\ \theta = \frac{1}{\beta n} \tag{3.2}$$

The greater the velocity of the particle, the greater the Čerenkov angle. The maximum angle occurs when $\beta = 1$ and is given by cos $\theta_{max}$=$1/n$.

The number of photons produced per unit path length is dependent on the particles velocity, the index of refraction of the medium and is given by

$$\frac{dN}{dx} = 4\pi^2 \int \frac{e^2}{hc\lambda^2}(1 - \frac{1}{\beta^2 n^2})d\lambda \tag{3.3}$$

As one can see in Equation 3.3, the number of photons produced is greatest in the low wavelength regime.

When choosing a radiator gas for the detector, one must consider all of these variables. One must choose a gas that has a sufficiently high index of refraction to produce many photons, but not so high that many pions will

from radiate. The gas should be transparent as far into the VUV as possible to increase the number of photons detected.

## 3.2 Photoelectric Effect

After Čerenkov photons are produced in the radiator gas, they must be detected. If photons of sufficiently high energy (frequency) strikes a photosensitive surface, an electron may be liberated as follows:

$$E = h\nu - W \tag{3.4}$$

Here E is the energy of the liberated electron, $\nu$ is the photons frequency, and W is the work function of the photosensitive material. As the equation shows, a certain minimum frequency is necessary to release the electron.

The photosensitive material in our detector was a CsI surface. A photon will liberate an electron from CsI if photons have a wavelength of roughly 200nm or less.

The probability of liberation on electron from a photo-sensitive surface is called $quantum\ efficiency$, QE($\lambda$).

$$QE(\lambda) = \frac{N_{electrons\ released}}{N_{incident\ photons}} \tag{3.5}$$

The QE has a strong dependence on the wavelength $\lambda$ of the incident light and is frequently presented as a percentage.

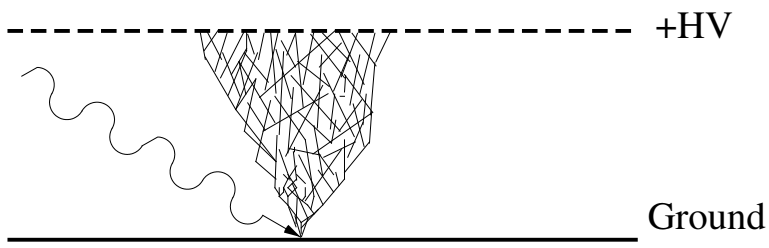


Figure 3.2: Schematic of avalanche. A photon strikes the photosensitive surface and releases an electron. This electron will accelerate towards the anode liberating additional electrons upon subsequent collisions with gas molecules.

## 3.3 Parallel Plate Avalanche Chamber

Once an electron is liberated from the CsI surface, it must be detected. The surge of current associated with the removal of a single electron is too small to be detected except under special circumstances. Our electronics require a surge of at least $10^4$ electrons to produce a signal above noise. This multiplication of a single electron into a detectable signal is done by avalanching it towards an anode.

### 3.3.1 The Avalanche

A Parallel Plate Avalanche Chamber (PPAC) is formed between two parallel conducting surfaces (plates) separated by a small distance (1-4mm). These plates are held at high voltage differences (usually one at ground and the other at positive high voltage) so as to create a large electric field between

them. If an electron is liberated between the two plates, it will accelerate towards the anode (+). If the electron gains sufficient energy, it will liberate additional electrons upon subsequent collisions with gas molecules. For PPAC, this avalanche is started the moment the electron is released from the CsI surface.

## 3.4 Energy Loss and Ionization

As a high energy charged particle travels through a material, it will experience an energy loss as it reacts with the molecules in that material due to inelastic collisions with the gas molecule's electrons and elastic scattering from the molecules nuclei. The amount of energy lost depends on the material in which the particle is traveling and the length it travels. The major part of the loss is due to the atomic electron collisions.

These inelastic collisions can be divided into two groups. The first is a soft collision in which there is only an excitation of the atom or molecule. The second type is the hard collision in which there is sufficient energy transfered to cause an ionization. In some of these hard collisions, there could be enough energy transfered that the liberated electron for it to cause secondary ionization. These high-energy liberated electrons are called $\delta - rays$ and can sometimes be troublesome is some detectors.

Thus as a high energy charged particle travels through a material, it experiences an energy loss. The average energy loss $dE/dx$, or stopping power, of a charged particle with a mass greater than that of an electron can be

calculated using $Bethe - Blochformula$ [24]

$$-\frac{dE}{dx} = 2\pi \mathrm{N_A} r_e^2 m_e c^2 \rho \frac{Zz^2}{A\beta^2}\left[ln\left(\frac{2m_e\gamma^2\nu^2 W_{MAX}}{I^2}\right) - 2\beta^2 - \delta - 2\frac{C}{Z}\right] \quad (3.6)$$

Here $m_e$ and $r_e$ are the electron mass and classical radius, $\beta = v/c$, $\gamma = \frac{1}{\sqrt{1-\beta^2}}$, $z$ and $v$ are the charge and velocity of the incident particle, $\mathrm{N_A}$ is Avogadro's number, $Z$ and $A$ are atomic and mass number of the atoms of the medium, $\rho$ is the density of the medium, $x$ is the path length in the medium, $I$ is the mean excitation potential, $\delta$ is the density effect correction and $W_{max}$ is maximum energy transfer in a single collision [31, 24]. The maximum energy transfer is produced by the $\delta - ray$ collisions. So for a particle with mass, M, [24]

$$W_{MAX} = \frac{2m_e c^2(\beta\gamma)^2}{1 + 2\frac{m_e}{M}\sqrt{1+(\beta\gamma)^2} + (\frac{m_e}{M})^2} \quad (3.7)$$

For the HBD, an avalanche gas with a very low $dE/dx$ is desirable to minimize the signal from non-electron particles.

## 3.5 Radiation Length

The radiation length $X_o$ of a material is the distance over which an electron loses all but $1/e$ of its original energy by bremsstrahlung (radiation loss only)[31].

$$\frac{1}{X_o} = 4\alpha r_e^2 \frac{\mathrm{N_A}}{\mathrm{A}}\left[Z^2(L_{rad} - f(Z)) + ZL^*_{rad}\right] \quad (3.8)$$

Where $L_{rad} = ln(184.15Z^{-1/3})$, $L^*_{rad} = ln(1194Z^{-2/3})$, $r_e$ is the classical electron radius, $\mathrm{N_A}$ is Avogadro's number, A is the atomic mass, $Z$ is the atomic

number, $\alpha$ is the fine structure constant, and $f(Z)$ is an infinite sum which can be approximated by

$$f(Z) = a^2[(1+a^2)^{-1} + 0.20206 - 0.0369a^2 + 0.0083a^4 - 0.002a^6] \qquad (3.9)$$

where $a = \alpha$Z.

For the HBD, the radiation length had to be kept to a minimum to minimize the number of reaction which may occur in the detector. This is extremely important, at PHENIX, since all but one detector are located behind the HBD.

# Chapter 4

# Preliminary Work

Before the HBD could be successfully built, a series of tests were needed. The tests were performed using a small single channel PPAC prototype. Additionally, the techniques for making high quantum efficiency cathodes needed to be developed.

## 4.1 Prototype Photo Detector Design

The small prototype photon detector consists of a photosensitive PPAC housed in an aluminum high vacuum vessel with a $MgF_2$ window as shown in Figure 4.1. The vessel was leak tested using a helium leak detector set to its most sensitive setting ($10^{-9}$ cc/sec). No leaks were detected. The cathode of the PPAC was a 3/16 Al plate which was machined flat and then polished smooth. The Al plate was then deposited with a 5000Å thick CsI layer.

The anode was a stainless steel mesh which was held in place by soldering(described later) it to a Cu clad G10 circuit card which was 1.5mm thick.

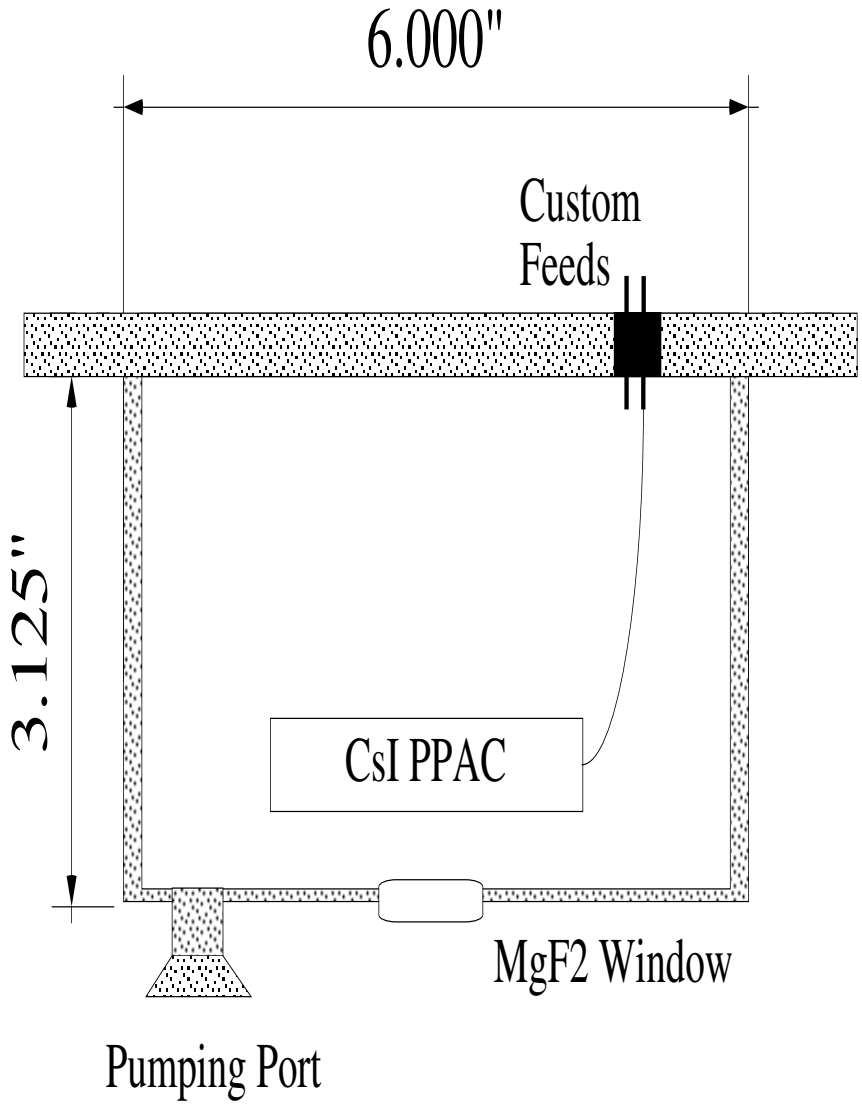


Figure 4.1: Shown is the small photon detector used for CsI cathode development and avalanche gas selection.

The circuit card provided the gap for the PPAC. On the back of the Al plate, a Minco thermo-foil heater was attached along with a thermocouple. The cathode was permanently attached to the back flange of the vacuum vessel and electrically isolated from the Al vessel. During evaporation the mesh was the only item removed. This design is essential to reduce the fresh CsI exposures in air via its rapid assembly (roughly 2.5 min).

### 4.1.1 Components and developed techniques

#### Magnesium Fluoride Window

The magnesium fluoride windows used for the small prototype were salvaged from a previous detector. The original detector had a 4.5" by 4.5" window that was 6mm thick. The windows were held in place using 3M Scotch-Weld DP-460 epoxy adhesive. This epoxy is dissolve using heavy duty paint stripper (like Klean-Strip KS-3 paint stripper.). Once removed from the old detector assembly, two windows windows were sent to Optovac in Boston, MA where the crystals were cut into several 1 inch round windows and re-polished for optimum VUV transmission. The round window was then epoxied to the small vessel. Other windows were lated epoxied to a bored out Conflat flange to be used when testing the final CsI detector.

$MgF_2$ has good transmission to about 120nm and nearly 100% transmission at the 180-200 nm wavelength where the quantum efficiency measurements were made.

**Anode Mesh**

The material used for the anode of both detectors was provided by David Anderson from the Particle Detector Group (PDG) at Fermi National Accelerator Laboratory (FNAL). The anode was a stainless steel mesh that had 50 micron wires with 500 micron spacing. This combination gave the mesh 81% light transmission. It is important that the anode mesh be mounted with sufficient tension to prevent it from sagging under the electric fields produced in the PPAC region. To insure high tension, the grid was stretched across a Cu-clad G10 ring using a Cam-Lok stainless steel stretcher from American M&M in Morton Grove, IL. The mesh was then attached using a 95% tin-5% antimony solder with HCl acid flux. This solder and flux worked extremely well with the stainless steel mesh. After soldering, the flux had to be neutralized by rising the mesh under water and the rinsing it with dehydrated ethanol.

### 4.1.2 Signal Feedthroughs

One concern which developed during the early stages of the project was how to bring the signals from the photon detector through the radiator vessel. Often this is done using hermetic BNC connectors. This, however, is very costly (48 connectors at ~$5 each) and would take up a great deal of space on the vessel back flange.

We decided to develop and test a custom feethrough for our application. The feedthroughs used are straight dual row headers manufactures by 3M

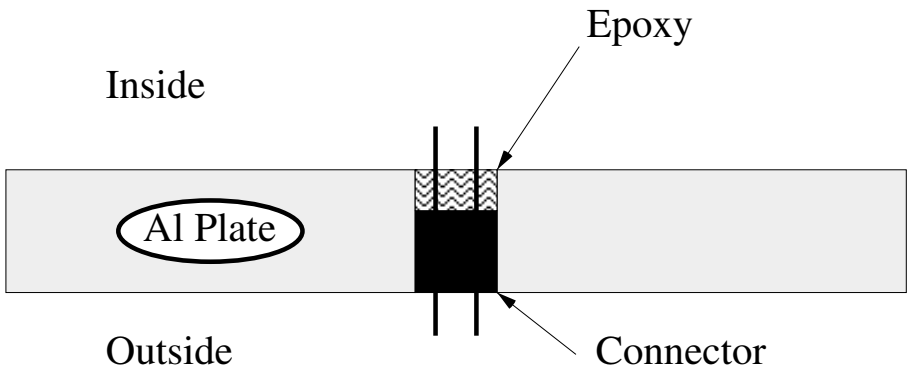


Figure 4.2: Shown is the custom feedthroughs developed for the HBD. Once the epoxy cures, the feed is durable and hermetic.

---

(supplier- Newark Electronics #44F7490 or 46F4425) with extra long pins cut to the desired length. In the small test vessel, a 10 pin connector was used. To install it, the following steps were followed

1. Cut connector to desired length.

2. Machine a groove of the proper width and length so that the connector would fit snug.

3. Clean all components thoroughly with ethanol.

4. Push the connector (long pins inward) into the grove making the connector front flush with the *outside* of the vessel.

5. Pour low out-gassing epoxy (3M Scotch-Weld DP-460 epoxy) to fill the grove from the inside being sure that the epoxy is making contact with

all the pins. At least .25 inch of the pins should be left exposed to make connections to.

6. Let the glue set and then test the connector for leaks.

A diagram of this is shown in figure 4.2. Roughly six connectors have been made and all have been helium leak tested to be hermetic even after numerous cycles of pumping and mechanical strain. These connector feedtroughs have also be adopted for use as the feedthroughs for the PHENIX RICH PMT array.

## 4.2 CsI Deposition

For prior chambers built by Dr. Hemmick group, the CsI depositions were performed at Fermi Lab by the FNAL Particle Detector Group. For the Hadron Blind Detector, it was decided that CsI evaporation would be done at Stony Brook for convince and experience. The CsI deposition was performed at Stony Brook. Our techniques are based identically upon the prescriptions set by Simon Kwan and David Anderson[17] of the Fermi National Accelerator Laboratory's Particle Detector Group.

### 4.2.1 The Evaporation

The bell jar used a large diffusion pump, which was protected against back flush of oil by a liquid nitrogen cold trap. Extensive cleaning of the bell jar was performed prior to our use. Cleaning consisted of scrubbing down every

surface in the bell jar with ethanol which typically took one person 4 hours to accomplish.

The surface of the cathode was cleaned with ethanol and the back plate (with the cathode already attached) was placed into the bell jar. The anode mesh, wrapped in foil, was placed at the bottom of the evaporator. This step was taken to help drive surface contaminants out of the G10 mesh support ring.

Evaporations were typically performed at a vacuum level of 7-8 x $10^{-8}$ torr which usually took 12-16 hours to achieve. During the pump down the cathode was gently warmed using the thermo-foil heated to between 55 and 60° C to help out-gas any contaminants on the cathode.

Once the proper pressure was reached the cathode's temperature was reduced to between 45 and 50° C. Roughly one watt of power to the heater produced these equilibrium temperatures. It is very important at this point that the temperature never goes above 55° C so as to prevent any additional out-gassing either during evaporation of the cathode or cathode operation

The CsI was evaporated directly from scintillator grade crystals (provided by David Anderson of FNAL)resting in a molybdenum boat. A movable shutter was placed above the boat. The shutter was closed as the boat was first warmed so that the initial deposition was only to the back of the shutter. This was to avoid evaporating surface contaminations from the CsI onto the cathode.

During evaporation, CsI was deposited simultaneously onto the cathode and a quartz crystal thickness monitor. A 5000Å continuous layer was de-

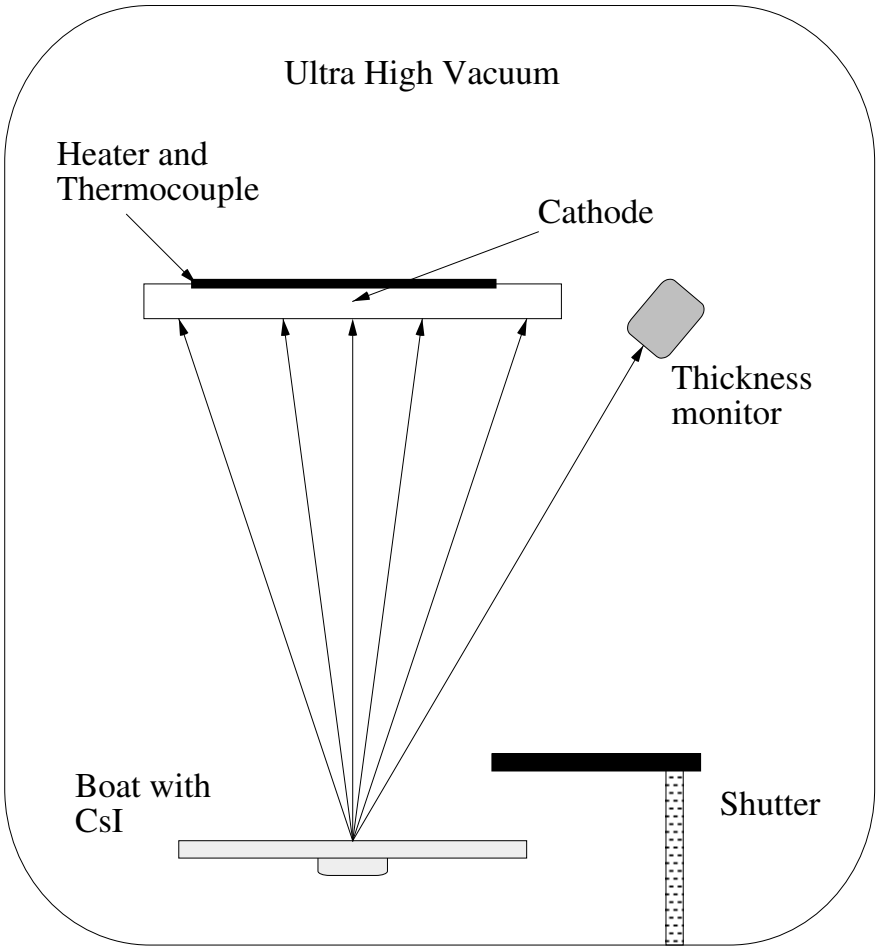


Figure 4.3: Schematic of evaporator used for CsI depositions.

posited in roughly 90 seconds (50 to 55 $\mathring{A}/sec$). The thickness was monitored by measuring the change in frequency of the crystal. A change of 11250 Hz was calculated to be roughly 5000Å using the following relationship

$$frequency \sim \frac{\mathring{A}}{2}\delta \tag{4.1}$$

Here $\delta$ is the density of the material being evaporated. 5000Å was chosen for the thickness since it has been measured that thicker coatings do not increase the quantum efficiency [29, 17].

After deposition, the evaporator was let up to UHP grade nitrogen. The cathode remained heated and warm during this procedure (45 to 50° C) and was removed warm from the bell jar. We believe that the warmth significantly retards condensation during the time that the cathode is handled in air. Once out of the bell jar, the anode mesh was put in place and the detector was assembled and pumped down. Total air exposure was typically 2.5 minutes.

Once pumped down to below a millitorr with a turbo pump, the cathode was heated to 50° C overnight. This is believed to improve the performance of the cathode by driving off surface contamination (water) which accumulated during assembly.

To date I have performed nine evaporations each of which was measured to have a quantum efficiency consistent with previous published results.

# Chapter 5

# Quantum Efficiency Of the Cathodes

The purpose of the QE measurement is to determine the quality of the cathode. We are not equipped to measure the absolute QE of the cathode to better than 20% systematic uncertainty. However, we can compare our cathode quality with those made for us by the Particle Detector Group (PDG) Fermi National Laboratory (FNAL)with high precision. To date all except the first of the cathodes was measured to have a quantum efficiency equal to those made for us in the past by the PDG at FNAL (see below).

## 5.1 Experimental Setup

### 5.1.1 Pumping Station

Although the HBD is operated at one atmosphere internal pressure, a vacuum system was necessary. First it was needed in testing the quantum efficiency QE of the cathodes. QE measurements are made at roughly 35 torr ethane to ease comparison to the FNAL cathodes. Second, it was needed to

evacuate the final HBD system once it was assembled.

The pumping station consisted of a 150 liter/sec turbo pump (Pfeiffer TPC 110) backed by a roughing pump. Pressure was measured with a thermocouple gauge and a capacitance manometer. The system is assembled on a movable rack since it is transported from the Stony Brook to a test Beam annually.

### 5.1.2 Flash Lamp

A Hamamatsu Xe flash lamp was used as a single photon source for the QE measurements. Figure 5.1 shows the schematic of the lamp system. Wavelength selection attenuation was done using an Oriel 77250 monochromator whose grating had a line density of 1200/mm which gave it tuneability from 175nm to 1000nm in increments of 0.2nm [49]. A 200nm band pass filter was placed before the opening of the monochromator to avoid light from higher order refractions. The light transition function is Gaussian with a sigma of 5 nm.

In order to achieve less than one photon per flash of the lamp, many attenuation factors were used.

1. The lamp DC power supply was set to 8 volts (1/3 its normal operating voltage)

2. The lamp was placed far from the narrow entrance slit of the monochromator

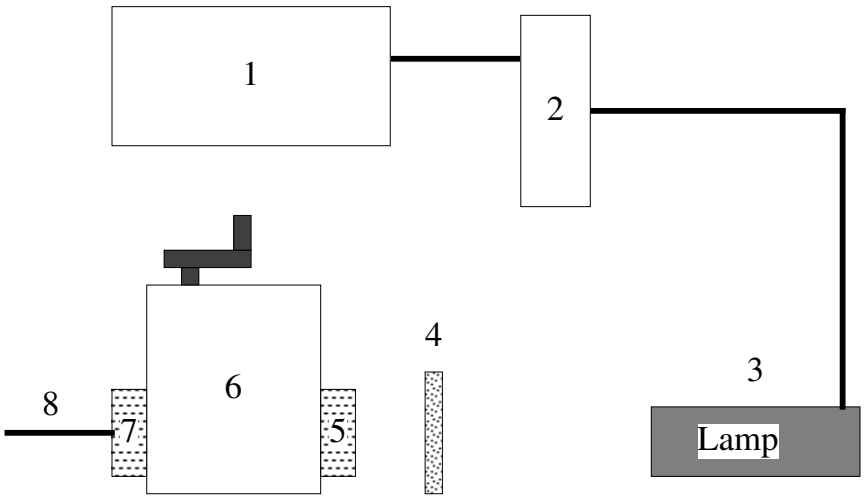


Figure 5.1: Schematic of the light system: (1) DC power supply; (2) HV-supply for the Xe-flash lamp; (3) Xe-flash lamp; (4) 200nm bandpass filter; (5) entrance slit; (6) monochromator; (7) exit slit; (8) quartz optical fiber.

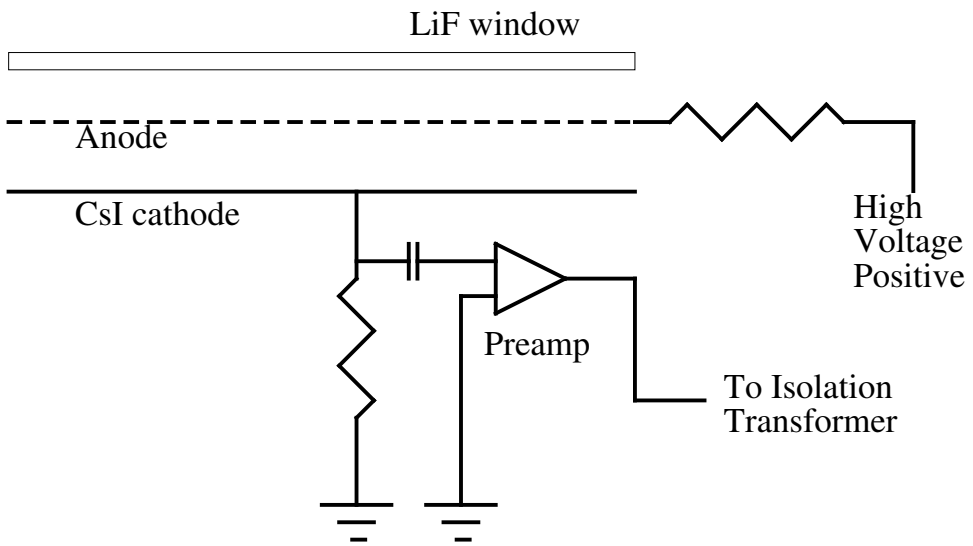


Figure 5.2: Figure shows the electrics used to digitize a signal from the PPAC

---

3. Attenuation occured in the air and the quartz optical fiber.

4. Very thin entrance and exit slits were selected on the monochrometer.

5. The final attenuation stop involved the strongly wavelength dependent transmission of various system components (air, quartz, bandpass filter)

6. By tuning the wavelength, one was able to effectively adjust the light intensity down to the measurement range of roughly .1 photo-electrons per flash of the lamp.

The light was carried from the monochrometer by a quartz fiber optic cable and sent to a photomultiplier tube (Hamamatsu PMT R166UH) or to the UV CsI chamber.

### 5.1.3 Electronics

The electronics used for the bench tests are the same as those that are used for the beam tests. They will be discussed in greater detail in later chapter. Here I will just give a brief description of them and how they were used for the bench test.

#### Brief description of electronic chain

The signal from the PPAC was first fed to a hybrid charge sensitive preamplifier through the custom feedthough. The signal from the preamp was then fed through an isolation transformer and then to a 250 nanosecond bipolar shaping amplifier. After shaping the signal was sent to a LeCroy model 2249W ADC. Figure 5.2 shows a schematic of the electronics connected to the UV chamber.

The signal from the PMT was sent directly to the same ADC as the UV chamber.

### 5.1.4 Bench Triggering

Figure 5.3 shows the trigger system for the bench tests. The initial pulse was made by a pulser. The trigger output was fed to the flash lamp while the pulse out put was fed into one port of a LeCroy model 222 Dual Gate generator. The output of that gate was fed to the other port. This allowed the first gate to act as a variable delay for the system. The second gate controlled the width of the gate which was fed to the ADC gate.

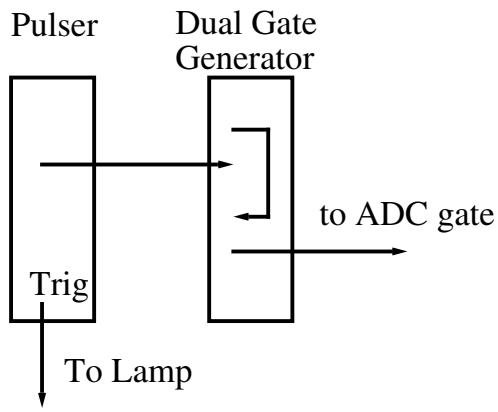


Figure 5.3: Diagram of bench trigger.

## 5.2 Measurements

The purpose of the QE measurement was to determine whether that cathodes made at Stony Brook were of the same quality as those made at FNAL in previous years. To do this, the identical method used to measure the FNAL cathodes was repeated.

Single photon signals from the flash lamp were achieved statistically by attenuating the Xe-flash lamp (as described in section 5.1.2) until the mean number of photon-electrons per pulse was roughly 1 in 10. The mean number of photon-electrons was determined assuming Poisson statistics and using the following equation

$$MEAN = -ln\left(\frac{N_{pedestal}}{N_{total\ number}}\right) \tag{5.1}$$

The QE reference for the CsI cathode was a CsTe photomultiplier tube PMT

(Hamamatsu model RU166UH). The QE of the PMT was taken from the catalog value and was roughly 40% at 187nm. Although it is well known that the quantum efficiency can vary dramatically on a tube-by-tube basis, reflective cathode tubes (such as ours) vary less in quantum efficiency than transmission style cathodes. We quote a 25% systematic uncertainty in the reference on the advice of the manufacture.

The CsI chamber was evacuated and then let up to 35 Torr of research grade ethane (99.95%). Five thousand events (one event per flash) were taken for both the chamber and the PMT at a wavelength of 187nm. Background runs with the lamp blocked( but not off) were then taken to determine the level of any stray light entering the system. The QE was determined by comparing the response of the CsI chamber with that of the PMT. Using the equation

$$QE_{chamber} = QE_{PMT} * \frac{MEAN_{chamber}}{MEAN_{PMT}} \tag{5.2}$$

where $MEAN_{chamber}$ and $MEAN_{PMT}$ are the mean number of photo-electron measured, the QE of the chamber can be determined.

**Results**

Several measurements on each cathode was made to confirm the reproducibility of the result. All except the very first cathode made had QE ranging from 21- 23 % at 187nm. This is in very good agreement with the results in the past from cathodes manufactures for us by the PDG at FNAL. Those cathodes were measured to have QE ranging between 20-25% at 188nm. We conclude

that the quality of the cathodes made by us at Stony Brook is equivalent to that achieved at FNAL.

# Chapter 6

# Additional Bench Tests

In addition to QE measurements, the small prototype vessel was used to test several other aspects of the HBD performance prior to assembly of the main detector. Among these were the avalanche gas mixture tests and the PPAC gap distance verse voltage holding capability.

## 6.1 Avalanche Gas Mixture

Originally it was hoped that a $He + .3\% CF_4$ mixture for avalanche gas as prescribed by Giomataris and Charpak [39]. This gas mixture has a very small $dE/dx$ and a wavelength cut off at about 106nm.

Our tests, however, showed that even at low concentration, the $CF_4$ still acted to steal the signal. The pulse height resulting from a single photon avalanche using a 5% $CF_4$ mixture was among the largest signals of the signals measured, however, the quantum efficiency was lowered to 4%, a loss of a factor of roughly six . One cathode was tested with ethane, then $He$+5% $CF_4$ and

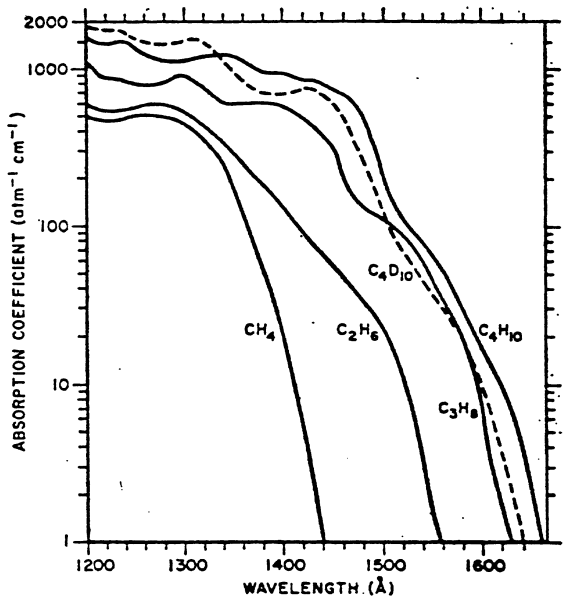


Figure 6.1: Absorption curves for hydrocarbons.[34]

---

then again with ethane. The QE dropped from 22% to 4%, and returned to 15% after re-introduction of ethane at 35 Torr. Although different electric field strengths should minimize the electron capture probability, further tests with $CF_4$ were not pursued.

Instead, we began a search for a possible replacement avalanche gas mixture. Helium is an optimal choice for the principle component of the radiator gas due to its small $dE/dx$ which minimizes the signal from non-radiating charged particles. A number of possible quenchers were tried in the hope of finding a mixture with transparency down to 120 nm. Such gases include nitrogen, carbon dioxide and hydrogen. All were unsatisfactory (gain less than

$10^4$ or wavelength cut off too high).

Our final choice for the avalanche gas was $He + 5\%\ CH_4$ since methane is the most transparent of the hydrocarbons (down to 140 nm at our low concentration and short detector length)[34]. Helium is quite easy to quench since the principle photon feedback lines are deep in the VUV, near 65 nm wavelength. Methane in concentrations as low as 1% yields a high gain avalanche and stable operation.

The $dE/dx$ of this mixture is low. We calculate that the mixture would liberate roughly .25 free electrons within a region that would produce a measurable signal from our electronics.

**Some Concerns**

It has been known for some time that the use of a noble gas in the avalanche mixture can have detrimental effects on the net quantum efficiency of the cathode (a factor of 4–10 reduction)[47]. This effect has been primarily associated with the reflection of the photo-electron back into the cathode via elastic collisions with the noble gas atoms. These effects have been specifically observed in association with CsI cathodes[13, 14], leading us to expect similarly poor results with our He based mixture. In all those tests, [47, 13, 14] the current produced from the cathode was measured under exposure to a (relatively) bright light source with the cathode under low electric field. We have performed tests of the cathode quantum efficiency in the presence of a noble gas mixture using the single photo-electron approach described above (high electric field).

We first measured the quantum efficiency of a cathode using pure ethane as the avalanche gas. This particular gas choice gives an especially high gain since it is more strongly quenched than pure methane and thereby a small systematic uncertainty in the photo-electro yield. The vessel was then evacuated and filled with the 95% He+5% methane mixture. We measured the quantum efficiency to be reduced by only 10% while using the noble gas mixture.

At first, the difference between our result and those previously cited seems surprising. Although the explanation is not completely clear, we would like to suggest a possibility based upon the simple model presented in reference [47]. There, electron collisions with a noble gas atom are compared to collisions of a small ball with a large hard sphere. Classically, one half of such collisions would result in a "back-scattering" of the incident, light electron. The analogy to a strong electric field is a severely tilted floor upon which only *directly backward* smatterings of the small spheres reflect them to their starting point. Although this is clearly an incomplete argument, it would suggest that the noble gas effect would be lessened in the presence of a strong electric field (800V/mm). We suggest that the strong electric field which exists at the cathode in a PPAC under full gain (sufficient to create a strong avalanche in the He mixture) may compensate for the reflection and restore the quantum efficiency.

## 6.2 Radiator gas

We had originally planned to use $CF_4$ as a radiator gas for the HBD. This gas had a good index of refraction (1.00062) and a wavelength cut off of

106nm. This would provide us with many photon-electrons. We discovered, however, that $CF_4$ produces scintillation light which would give pions a signal. We calculated that less than .5 photons would hit the HBD cathodes surface per pion. This would be fine for the prototype, but in the actual upgrade detector this would be a problem because the detector would be covering a very large area.

We decided to instead use $C_2F_6$ as the radiator gas. This gas has a higher index of refraction than $CF_4$ and a factor of 40 less scintillation light. The wavelength cut off was 130nm however. This cut off does not effect us since our wavelength limiting factor was the avalanche gas mixture at 140 nm.

## 6.3 PPAC Conditions

Originally we had planned to use a gap of 4mm. Later it was decided to reduce this gap as much as possible. This would to reduce the amount of ionization created in the PPAC region by charged particles like pions. The gap chosen for the small prototype was 1.6mm. In our tests, this gap proved to be more than sufficient to produce the gain necessary for our electronics. The high voltage HV for this gap at atmosphere ranged from 800-1000 volts depending on the percentage of methane used in the mixture.

# Chapter 7

# Hadron Blind Detector Design

In this chapter I will discuss the design of the HBD including the radiator vessel, CsI photon detector, PPAC assembly, and the gas flow topology. The radiator vessel and photon detector were both designed by me under the supervision of Dr. Thomas Hemmick. All aluminum parts except for the feedthrough on the back flange and the lower lid itself were machined by the Stony Brook Machine Shop. All other parts were machined by myself. All parts of the vessel and the photon detector were tested to be hermetic after assembly using a Helium leak detector.

## 7.1 Radiator Vessel

Shown in Figure 7.1 is the radiator vessel and gas flow diagram for the HBD. Figure 7.3 is a photo of the detector itself. A mixed beam of electrons and negative pions enters the detector from the right. The Radiator vessel contains two 1 meter long, 5 inch diameter stainless steel tubes with 6.75 inch

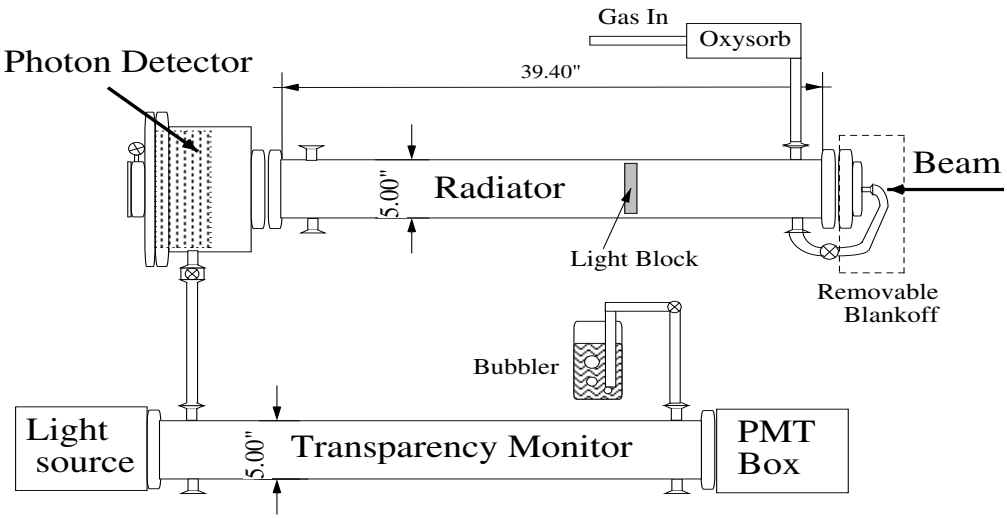


Figure 7.1: Hadron blind detector diagram showing Radiator vessel, transparency monitor, and radiator gas system.

---

ConFlat knife edge flanges on each side. Each tube has four quick connect fittings, two NW16 and two NW25 as shown. The tubes were manufactured by Varian Vacuum.

The detector housing is also shown in Figure 7.1. It is made from a 10.75 inch tube that is 8 inches long. It has a 6.75 inch ConFlat flange on the entrance side and a 13.25 inch ConFlat edge on the exit. Also located on the housing is a NW 25 Quick connect port. The photon detector is mounted on back flange of the housing. All the electrical and gas feeds for the photon detector pass through this end plate. A photo of the outside of the flange is shown in Figure 7.2.

The entrance and exit windows are made from 2 mil thick Kapton which

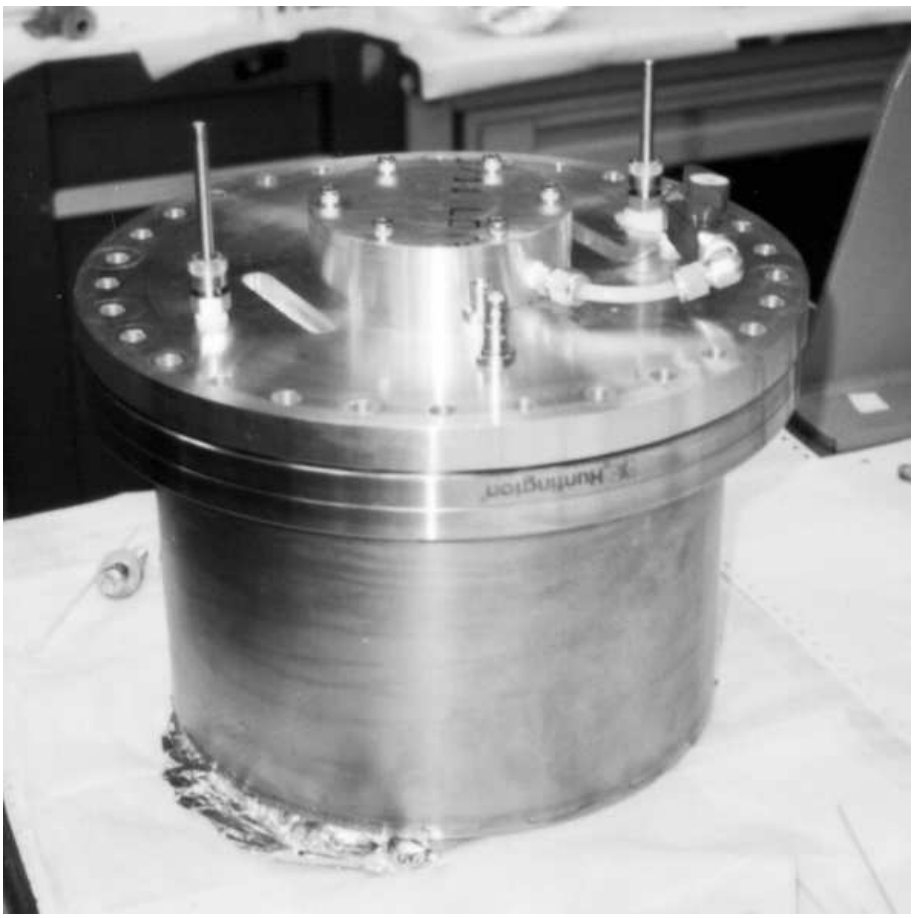

Figure 7.2: Back flange and Detector Housing. Shown are the Cajon ultra-torr fittings, the custom feeds(recessed in grooves), the SHV connector and the end blank-off with linking gas feeds.

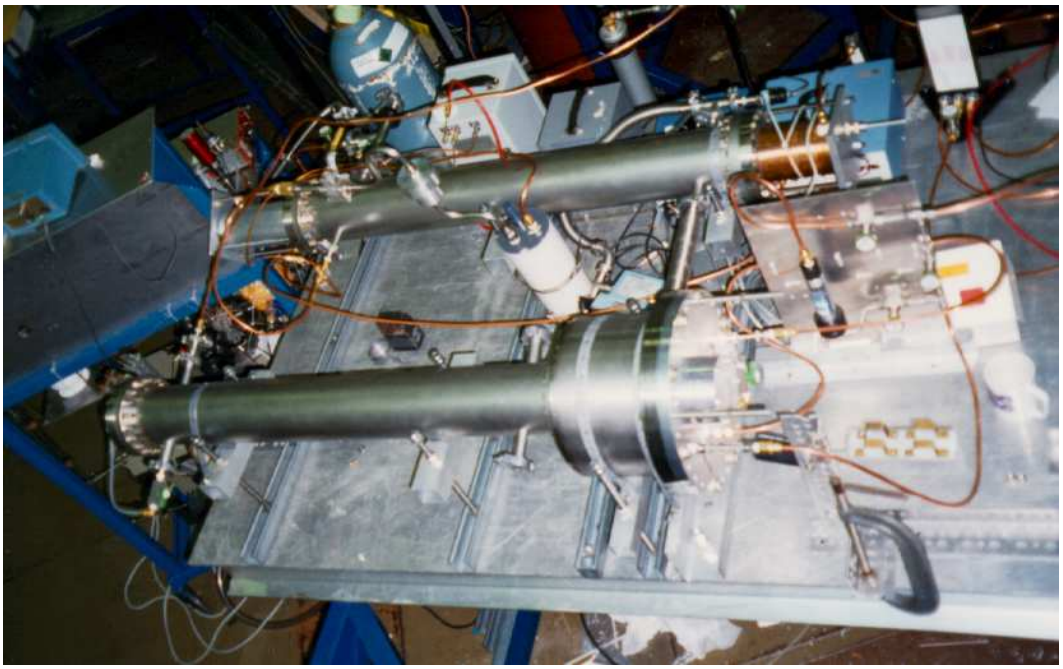

Figure 7.3: Hadron Blind Detector photo while in LINAC Assembly area.

is aluminumized on the interior side. Aluminization is necessary to prevent diffusion of water into the radiator gas and a subsequent loss in UV light transmission. The mounts for the radiator vessel windows accept exterior blank-offs for use when evacuating the vessel. The windows are pumped on both sides (exterior side through a valved line) to prevent implosion.

After entering the detector the beam passes through the radiator gas volume traveling toward the photon detector. A movable "sail" is placed in the radiator tube and acts as a light block. Only light created downstream of the sail can reach the photon detector. The sail is made from an aluminumized kapton foil mounted on a 4.5 inch diameter aluminum ring. The ring is

mounted onto an aluminum sled with strong magnet attached to the center of its base. This magnet allows the sail to be repositioned without breaking the radiator vessel seal by using a second magnet from the exterior of the radiator vessel.

The beam passes directly through the photon detector and exits through the Kapton exit window. The photon detector is mounted upon a large flange which acts as the back wall of the radiator vessel.

## 7.2 Gas Flow

High purity gas flows through a large Oxysorb cylinder prior to entry into the radiator vessel. The gas enters near the beam entrance, flows along the entire length of the radiator tube, and passes over the photon detector. After this, the gas passes through the transparency monitoring tube prior to bubbling through low vapor pressure Si diffusion pump oil and finally out to air. Radiator gas flowed at a rate of about 10 liters per minute while the avalanche gas mixtures flowed between 100 and 150 cc/min.

## 7.3 Support Equipment for Radiator Vessel

In order to operate the Hadron Blind Detector in the vacuum ultra violet (VUV) it must be pumped down to remove as much water, oxygen, and other contaminants as possible. Additionally, the quality of the gas needs to be monitored. A Meeco Inc moisture analyzer (model W) was connected to one of

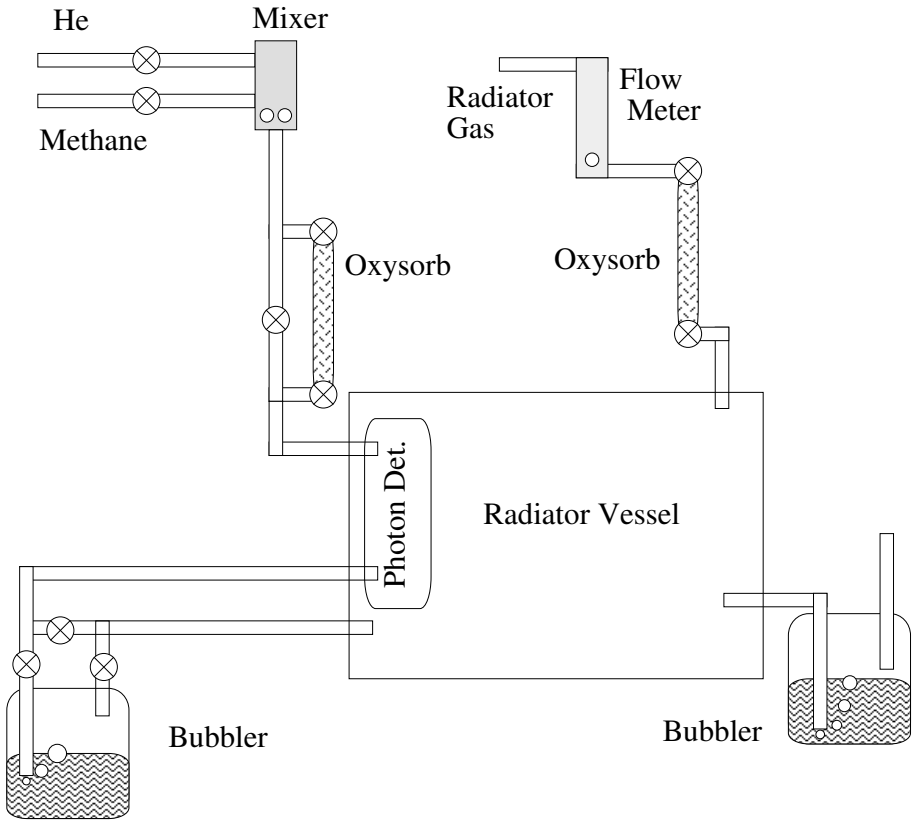


Figure 7.4: Hadron blind detector gas flow schematic for the avalanche and radiator regions.

the ports near the end of the TMS. This device measures water contamination with a sensitivity of one part per million. The analyzer continually measured the vessels the water contamination which was below 3ppm for all data runs.

All gases entering the system were always fed through Oxysorb canisters to reduce the water and oxygen contamination. The pressure difference between the vessel and its exterior was monitored by a Datametrics' Barocel Electron manometer (model 1174) which has millitorr precision. This difference in pressure was set by the depth of the Si oil in the bubbler and was typically 15 torr. A photo of some of the support equipment for the HBD is shown in Figure 7.5.

## 7.4 Transparency Monitor

The second tube in Figure 7.1 is the Transparency Monitoring System (TMS). It was used to periodically check the transparency of the radiator gas. VUV transmission in this part of the radiator vessel should be the worst in the system at this point. The ends of the TMS tube are blanked off with ConFlat blanks which have been bored out to accept a 1 inch round $MF_2$ window. The window was epoxied in place using 3M Scotch-Weld DP-460 epoxy adhesive.

A Hamamatsu Model L879-01 continuous $D_2$ lamp (with $MgF_2$ window) is mounted at one end of the TMS. The wavelength of light sent into the gas volume is selected using one of three narrow bandpass filters (124nm, 156nm 173nm, bandwidthsin +/-10nm purchased from Acton Research, Mass.). After passing through the TMS tube, the light level is measured by a photomultiplier

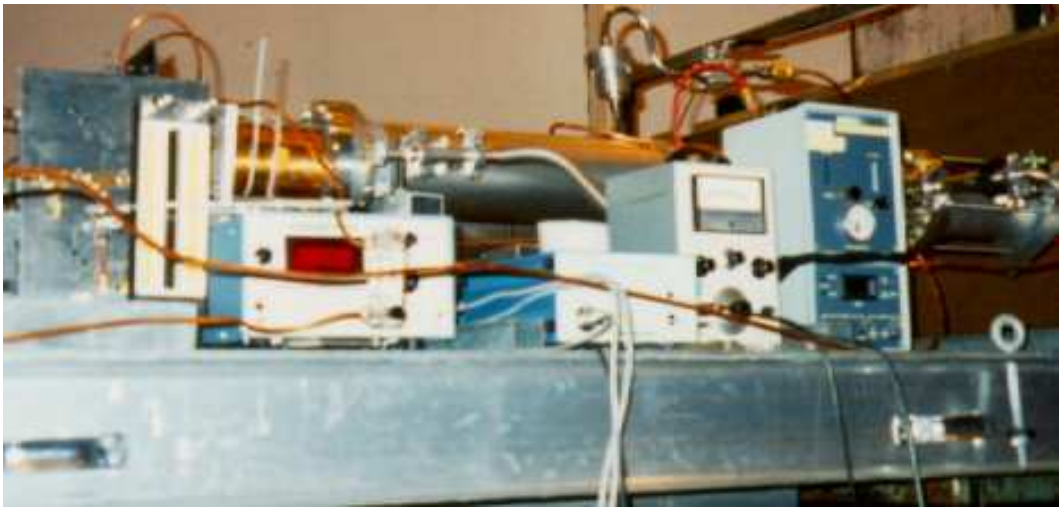

Figure 7.5: Photo shows the support equipment for the Radiator Vessel. From left to right:avalanche gas mixer, manometer controller, deuterium lamp power supply, the nanoAmp meter, and the water monitor.

---

tube which has a $MgF_2$ entrance window and bialkilide cathode. Transmission is measured by comparing the PMT current to that measured with the TMS tube under vacuum. Both the housing of the PMT and the lamp where kept under constant UHP nitrogen flow during their operation. This is done to displace the oxygen and water in the housing which would absorb the light in our wavelength region of interest. The gas flow also serves to cool the lamp.

## 7.5 Photon Detector

The design of the photon detector is driven by a variety of requirements. First and foremost is the requirement that the fragile LiF window not break.

Care must be taken to mount the window in a stress free manner as well as to ensure that no significant difference in pressure develops between the avalanche and radiator gas volumes. The design must allow for a quick detector assembly after evaporation to minimize exposure of the cathode to air[14]. The cathode plane must be low mass and quite flat. Additionally, the pad plane surface must be chemically compatible with the CsI coating excluding a simple Cu-clad PC board[18].

The photon detector is a disc that measures 10 inches in diameter and 2 inches in depth. An exploded view of the photon detector is shown in Figure 7.6. The beam enters from the top, passes sequentially through the LiF window, anode mesh, pad plane, and finally exits through the vessel back window. I will describe the detector from to bottom, or rather, from particle entrance to exit.

### 7.5.1 LiF Window Support

The design of the detector calls for a very thin window to separate the radiator gas from the avalanche gas. This window has to be very thin to minimize the radiation length of the detector and has to have very good transmission deep into the vacuum ultra violet. The crystal which was chosen to be used was LiF. LiF has transmission down to 120nm and has a long radiation length ($X_o$=14.91 cm) implying that a thin yet easily manufactured window would suit our needs. At 0.5mm thickness, the window would account for only .3% of a radiation length. The window was 12cm in diameter and was manufactured

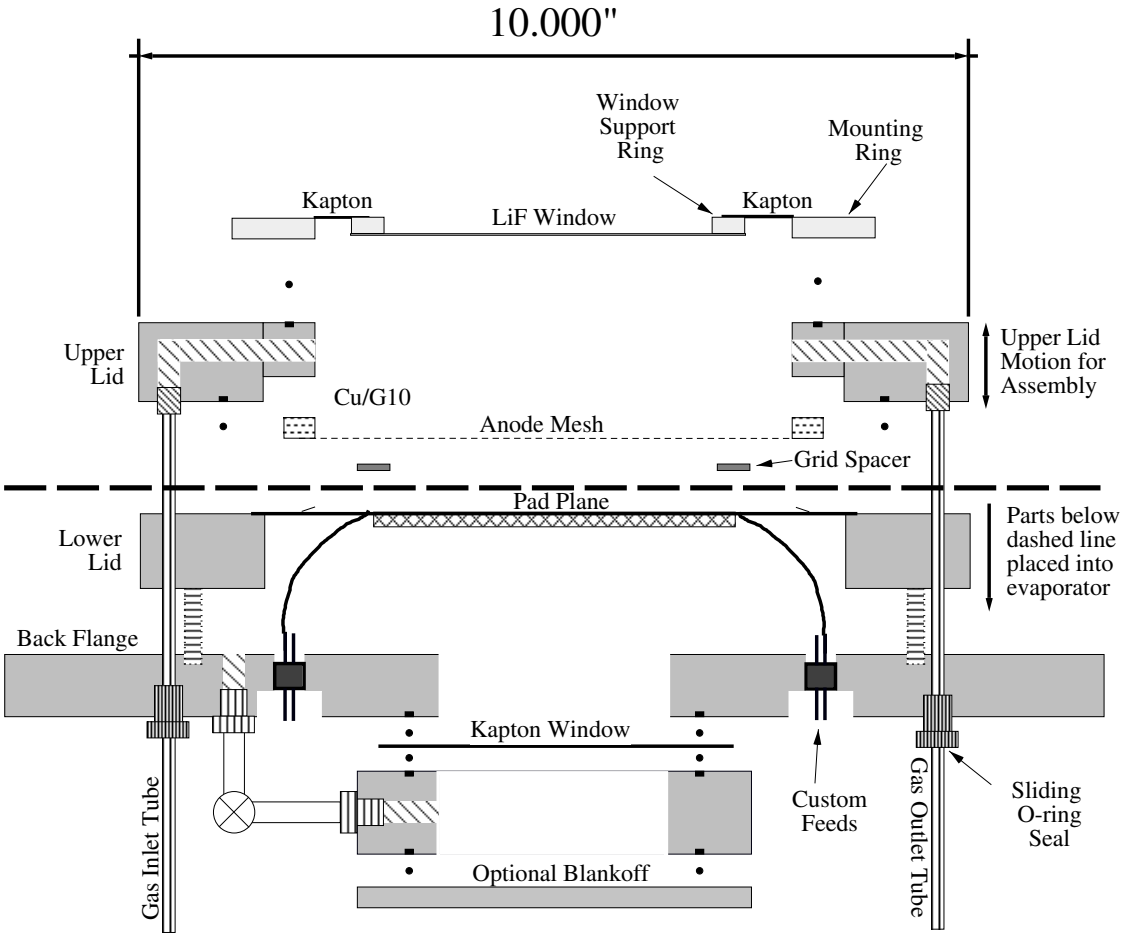


Figure 7.6: Expanded view of the components of the photon detector.

by OptoVac, inc. in Acton, MA. Three windows were ordered in total. Two that were 1 mm thick and one which was .5mm thick. The .5mm window was used in the final detector.

**"Stress-eliminating" support fixture**

Since the window was extremely fragile, a "stress-eliminating" support fixture was necessary to avoid breakage. The LiF is glued directly to the aluminum inner window support ring as shown in Figure 7.6. This inner ring was .1875 inches thick, had a 4.75 inch outer diameter (O.D.), and a 4 inch inner diameter (I.D.). The epoxy used was 3M Scotch-Weld DP-460 epoxy. A continuous bead of epoxy was made on the ring using a small (1mm thick) stick. It is very important that the bead is continuous so that the seal between the ring and the window is hermetic. Once the bead was put down, the LiF window was carefully lowered into place. (This is a one time step, since the surface tension of the epoxy on the window would surely break the window upon any attempts to remove it.) After the LiF is in place, another ring is placed on top of the crystal to apply slight pressure on it as the epoxy cures.

This window ring is connected to the rest of the photon detector by an aluminumized Kapton sheet. This sheet is stretched and epoxied to both the outer and inner window mounting rings. The outer ring is .25 inches thick, has a 5.75 inch I.D., and a 7.75 inch O.D.. The outer ring is shown in Figure 7.6. It is eventually bolted to the Upper Lid of the detector and makes a seal via an O-ring. The inner window support ring is then epoxied to the center of the Kapton sheet. After all epoxies have cured, the Kapton skeet which blocks

Figure 7.7: Photo shows the pad plane (top center), the upper lid (lower left)and lower lid (lower right) before detector assembly.

---

the LiF window is cut away.

In this "floating" configuration, stresses on the detector and the outer mounting ring result in twists or distortions of the Kapton and are not transferred to the LiF window. After the beam test was complete, a spare window mount was tapped forcefully and repeatedly against a table top. The window did not break.

### 7.5.2 Upper Lid

The window support structure is bolted to the Upper Lid. This upper lid provides the gas feeds into the cathode region. It is a 1 inch thick ring that has a 5.75 inch I.D. and a 10 inch O.D.. A figures of the upper lid

is shown in Figures 7.7 and 7.6. Two stainless steel 1/4 inch tubes were connected to the upper lid using NPT weld fitting. The tubes were 15 inches long and slid through the back flange through bored out Cajon Ultra-Torr fittings. The upper lid is designed to be slid into and out of place for the detector assembly/disassembly process.

### 7.5.3 Anode Mesh

The anode grid consists of a stainless steel mesh with 50 micron wires and 500 micron spacing (81% transmission). The grid is stretched across a Cu-clad G10 ring and attached using a 95% tin-5%antimony solder with HCl acid flux as described in Section 4.1.1. The Cu-clad ring was made from a .25 inch thick G10 circuit card. It was machined into a ring of 5.75 inch I.D. and a 6.5 inch O.D.. The cut edges of the G10 were painted with a low out-gassing epoxy to prevent the G10 from out-gassing.

### 7.5.4 Grid Spacer

The grid spacer is one of the most important pieces of the PPAC. It is a 1.6mm thick ring of Delryn. Its I.D. is 11.2 cm and has an O.D. of 13.8cm. The spacer was made slightly larger than the active area of the cathode plane to provide extra insulation for the signal strip located on the back of the circuit card.

The grid spacer is the only precision piece necessary for the PPAC. It is placed between the grid and the cathode plane. The spacer is held in place by

the friction induced by the mesh and the cathode pad plane.

**High Voltage**

High voltage (HV) contact is supplied by a set of four Au-plated spring contacts located around the perimeter of the pad plane. The spring contacts were connected to the pad plane with solder and were carried out of the detector through plated through holes which were sealed with solder.

### 7.5.5 Lower Lid

The lower lid serves as the support for the PPAC cathode plane. The lower lid is an aluminum ring 1 inch thick. It has a 5.75 inch I.D and a 10 inch O.D. It has a bolt hole arrangement that matches that that of the upper lid. Two of these holes were notched out to clear the weld fittings on the upper lid. A photograph of the Lower lid is shown in Figure 7.8. The lower lid is permanently bolted the the back Flange.

### 7.5.6 Pad Plane

The cathode pad plane is printed on a 6 mil thick double sided G10 circuit card ($\frac{1}{2}\frac{oz}{ft^2}$ ,0.0006" of Cu) on each side. Plated-through holes of 10 mil diameter carry the signals from the center of each pad to the back plane. Figure 7.9 shows a sketch of the cylindrically segmented pad plane. Not shown in the figure is the feedthroughs for the high voltage spring contacts which are located about 1.5 cm out from the outer most ring of the pad plane. The

Figure 7.8: Photo of the lower lid of the photon detector while being machines. Note the two notches which are used to pass the gas fittings through.

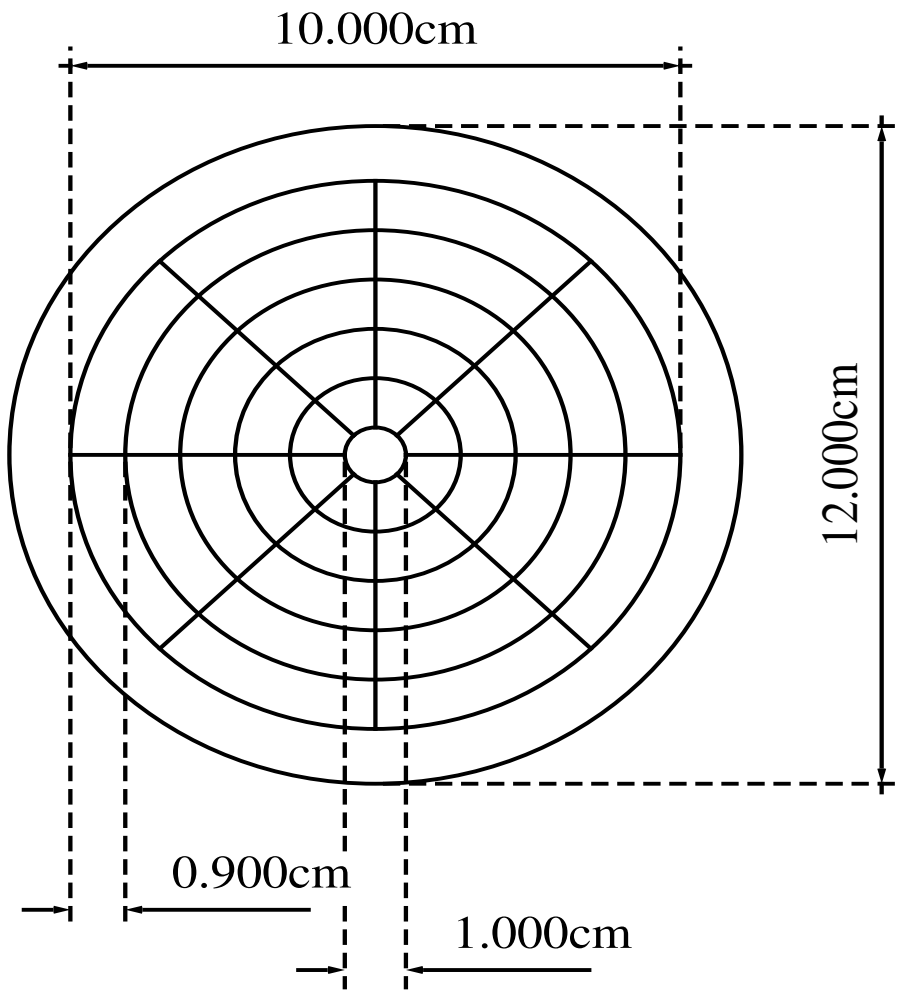


Figure 7.9: Sketch of the detector's pad plane showing pad segmentation

circuit diagrams were drawn up using E-Cam. The boards were manufactured by Accurate Circuit Engineering (ACE) in Santa Ana, Ca. A photo of the Pad Plane mounted to the lower lid and back flange is shown in Figure 7.10

It has long been known that a CsI coating deposited upon Cu will readily form CuI and perform with a substantially reduced quantum efficiency[18]. Cu pads with an electroplated layer of Au have also been shown to be problematic due to the diffusion of Cu through the Au layer [50]. Because of this, our pads used an electroless plating of Ni (2.5 micron) followed by an electroless plating of Au (0.125 micron) to become chemically compatible with the CsI layer. The Ni serves as a diffusion barrier to prevent migration of the Cu to the surface. The Au provides a chemically neutral substrate for the CsI layer. After the detector was assembled, an article was found that indicates that a smooth micro-topography of the CsI layer is critical to the performance of the cathode and that the Ni/Au substrate induces an especially smooth surface growth pattern[18].

The G10 circuit card of the pad plane was cut into a 19cm diameter disc. The circuit card was epoxied to the lower lid.

### 7.5.7 PPAC and CsI supporting material

A Minco Kapton foil heater is epoxied to the back of the pad plane. It is used to bake the cathode during and after evaporation. A thermocouple is inserted on the back of the heating foil. The heater is followed by a carbon fiber-epoxy hexcell honeycomb and then a backing of another 5 mil sheet of

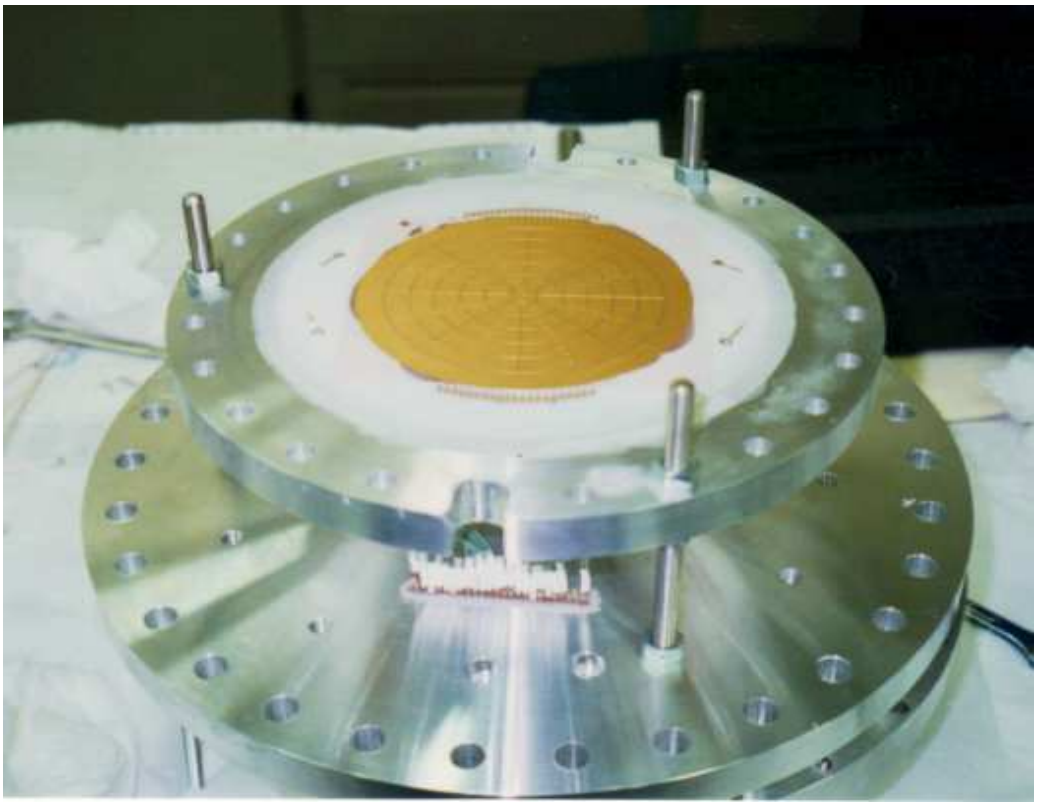

Figure 7.10: Photo of photon detector prior to being placed in the evaporator. Photo shows the pad plane, the HV contact springs, the lower lid, signal feeds and the back flange.

G10. During construction, the pad plane is placed face down on a flat granite table. After all parts have been epoxied (3M Scotch-Weld DP-460 epoxy) and put into place, a large weight is placed on the assembly until the epoxy sets. The hexcell sandwich serves to stiffen and flatten the pad plane without adding a significant amount of material to the detector.

Signals from the pad plane are connected to the custom feedthroughs by Teflon insulated wire. The wires are soldered to the back of the pad plane on the signal strip and then connected to the pin strip with gold pin connectors. Both the thermocouple and the foil heater are connected with Teflon wire and are also fed through the custom feedthroughs.

### 7.5.8 Back Flange

The actual photon detector is mounted on the back flange of the radiator vessel. A photo of this flange and the detector housing is shown in Figure 7.2. As shown, all the electrical and gas feeds go through the flange. Figure 7.11 shows the photon detector mounted to the back flange prior to its insertion into the housing. The electrical feeds are the 50 pin custom connectors as described in Section 4.1.2.

The gas to the CsI chamber is brought in through the stainless steel tubes which are welded to the upper lid. Seals against these tubes are made with bored out Cajon Ultra-Torr fittings. Located on the back flange is an hermetic SHV feedthrough for the high voltage along with a pair of custom 50 pin feeds. In the center of the flange is a removable blank-off which has a feed linking

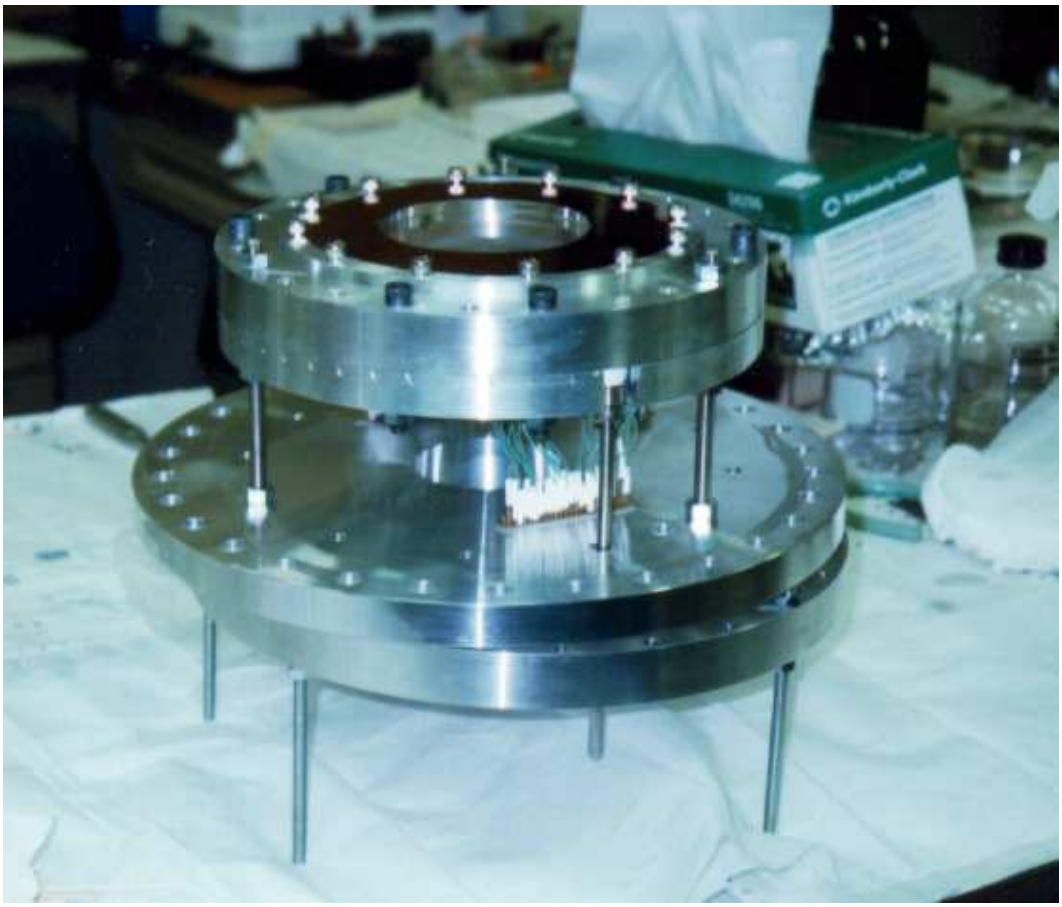

Figure 7.11: Photo shows the photon detector mounted to the Back Flange.

the interior of the vessel to the area in between the Kapton end window and the backplate. These volumes are connected during pump down and let up of the vessel. A valve isolates these regions when the blank-off is removed during beam tests.

## 7.6 PPAC Region

To make a properly functioning PPAC, it is imperative that the pad plane be not only flat but highly parallel to the HV grid. The grid cannot be permanently attached to the pad plane since it must be removed during the evaporation stage. However, if the anode mesh were attached instead to the upper lid, a large number of high precision pieces would have been necessary to ensure that the grid remained parallel to the pad plane. We have solved these problems using only a single precision piece: the grid spacer.

A diagram of the anode mesh , grid spacer, and pad plane in its assembled form is shown in Figure 7.12. The upper and lower lid are machined in such a way that the nominal spacing in the absence of the grid spacer would be 0.6 mm. The grid spacer piece (1.6 mm thick) is placed between the grid and pad plane. During assembly, the grid is gently stretched across the grid spacer ring and automatically adjusts to be exactly parallel to the pad plane. Additionally, we have engineered the pad plane's hexcell stiffener so that under the unavoidable stresses created during assembly, the active area will not distort. As shown in Figure 7.12, the hexcell stiffener is sized to completely cover the active area and the region below the grid spacer, but does not extend to the

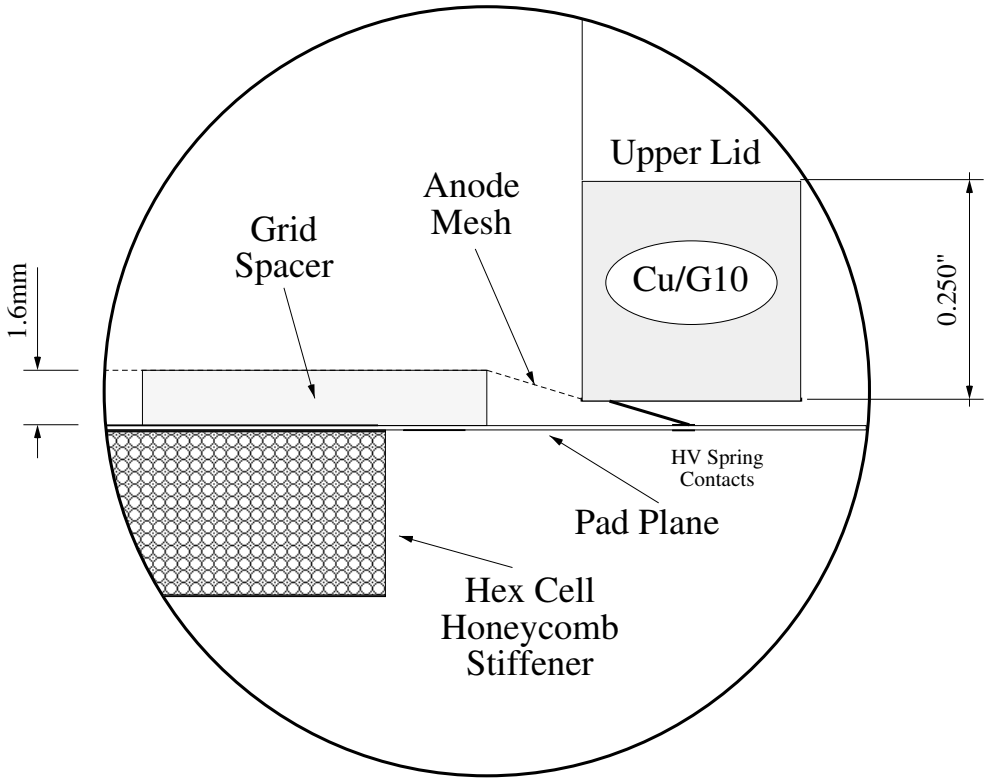


Figure 7.12: A sketch of the assembled PPAC region showing the grid spacer held in place creating the avalanche gap. It should be noted that the distance between the mesh mounting ring and the pad plane is less than the thickness of the grid spacer.

outer edge of the pad plane circuit card. In this way, the outer regions of the circuit card absorb all necessary deflections (HV contact springs, forces from grid spacer, gas pressure differences across the pad plane) leaving the active area quite flat. Thus, in some sense, the active area of the pad plane is also in a floating fixture similar to that of the window. These considerations were crucial to achieving the high gain and excellent uniformity discussed below.

## 7.7 Evaporation and Assembly

All items below the dashed line in Figure 7.6 are placed in the evaporator during deposition of the CsI layer. The lower lid is permanently attached to the back flange (which serves as the final seal of the radiator vessel). All signal connections are made (through to the feedthroughs) as well as high voltage, Kapton heater, and a thermo-couple. Quick assembly was aided by the configuration of the gas lines. Gas inlet and outlets flow through straight stainless steel tubes which are permanently attached to the upper lid as shown in Figure 7.6. During assembly the tubes are inserted through bored out Cajon Ultra-Torr fittings (O-ring seal on tube exterior) permanently mounted in the vessel back flange. Assembly after deposition involved the following steps:

1. Place grid spacer on pad plane.

2. Place anode mesh on spacer.

3. Place upper lid on anode mesh (LiF window already attached) and bolt in place.

Figure 7.13: The photon detector is suspended upside down in the evaporator while still attached to the back flange.

4. Insert completed detector into radiator vessel.

The entire procedure took less than 10 minutes using the real detector and including a 3 minute walk from the evaporator lab to the hall housing the radiator vessel. Both the photon detector and the radiator vessel were tested with a He leak detector and registered no leaks to its most sensitive setting ($10^{-9}$ cc/sec). A photo of the detector while in the evaporator is shown in Figure 7.13

## 7.8 Fabrication Issues

Several issues drove the design of the HBD. The outcome of these decisions were crucial to the current detectors design and success. We review here a brief history leading from the proposed design to the final working detector.

- **Vessel Design:** The original design for the vessel was to have a single tube about 24 inches in diameter. Located on the upper half of the tube would be the photon detector and on the lower a transparency monitor. This design was changes because of its volume. The radiator gas is very expensive. So, to keep within the budget of the project, the volume was reduced by instead making two small tubes. The reduction in size also reduced the cost of the fabrication of the vessel itself.

- **Pad Plane:** From the start, the pad plane was intended to be a circuit card. At first, many companies were contacted to see whither they could make plated through hole with Al. Aluminum was previously used for

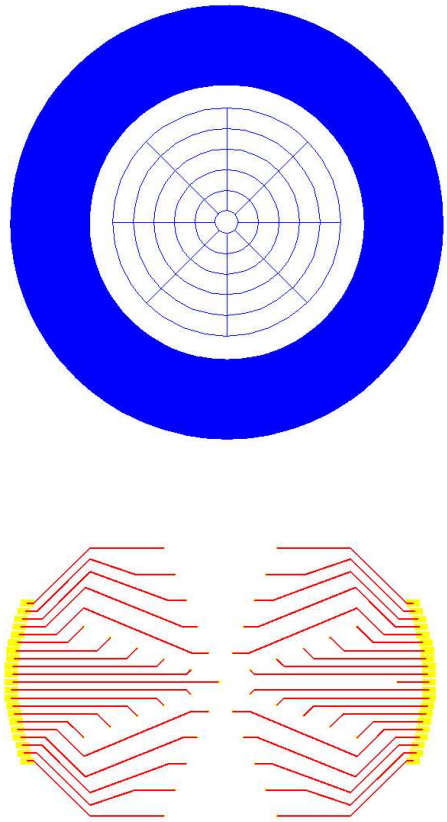

Figure 7.14: Front and back side of detector plane card showing cathode segmentation and wire traces.

cathodes and was found to be very stable with CsI. None of the companies, however, were able to make the card from Al. So our efforts shifted to a gold plated Cu card. It is known that CsI does not react with gold. After discussions with a company technician Alan Vogelstrum we chose to go with a gold/Ni plating procedure. The Ni acts as a barrier to prevent the Cu from migrating through the gold to the surface. The thickness of the Cu was also a consideration. Of course, the thinest possible layer is desirable. The pad plane for the HBD started as a $\frac{1}{2}\frac{oz}{ft^2}$ (0.0006") double sided G10 board. A thinner $\frac{1}{4}\frac{oz}{ft^2}$ is also made, but it is not always available. Ten mil holes were plated through which usually adds $\frac{3}{4}\frac{oz}{ft^2}$ during the plating process. The additional Cu from plating the hole was kept to a minimum while still insuring continuity. In doing this our boards had a final Cu thickness of .0013" on the pad plane. Figure 7.14 show the actual prints used to etch the front and back of the pad plane.

- **Window Material:** Although LiF was chosen for the window material of the HBD, $MgF_2$ was also considered. $MgF_2$ is 4 times harder than LiF and has transmission down to 120 as LiF. The reason it was not chosen however was because of its radiation length. In order to get .3% of a radiation length from $MgF_2$, the thickness of the window would need to be less than .25mm. This would not have been possible to manufacture. The polishing necessary to obtain VUV transmission would have destroyed a window that was that thin [33].

- **Radiation Thickness:** It was very important to keep the radiation thickness of the detector to a minimum. Table 7.1 shows the total material in the particles path. The Hexcell was ignored because of its very slim profile in the beam. The total radiation length for a 40cm would be 1.205% which is quite thin and would not pose a problem for PHENIX.

- **Gain Uniformity** The uniformity of the gain across the 12cm detector surface was inspected using the UV light source. Bright light flashes (thousands of photon-electrons per flash) were scanned across the entire surface of the detector. Response (the product of gain and quantum efficiency) was monitored by measuring the pulse height from the anode. A maximum variation of 10% was observed, an excellent result for a PPAC.

- **Čerenkov light in the window.** At normal incidence, Čerenkov light produced in the window is totally internally reflected and thus does not contribute to the pion signal. This is the case for the prototype detector tested. Such is not the case at non-normal incidence which would be the case in the actual HBD. Part of the Čerenkov cone will be transmitted through the window. The following factors should be considered when doing any calculations:

  1. The fraction of the Čerenkov photons which are not internally reflected varies as a function of particles incident angle.

| **Item** | **Thickness** | **Percent of $X_0$** |
|---|---|---|
| Cu pads | 1.3 mil | 0.231% |
| G10 | 10 mil | 0.130% |
| LiF | 0.5 mm | 0.300% |
| Kapton | 4 mil | 0.040% |
| Al(plating) | $100\mathring{A}$ | $10^{-5}$% |
| Heater | 2 mil | 0.080% |
| Ni | $100 \times 10^{-6}$ inch | 0.017% |
| Au | $1 \times 10^{-6}$ inch | 0.080% |
| CsI | 500 nm | 0.003% |
| SS grid (average) | 50 micron | 0.057% |
| $C_2F_6$ | 40 cm | 0.267% |
| *Total* | — | $\approx$1.205% $X_0$ Per Detector |

Table 7.1: Table shows the breakdown of the radiation percentages of the materials used for the detector.

2. The fraction of Čerenkov photons which penetrate the anode grid varies as a function of photon angle.
3. The distance over which the particle radiates (length of the medium) varies with incident angle (distance = thickness/cos($\theta$)).
4. The index of refraction in the window[48] and quantum efficiency of the cathode both vary as a function of wavelength.
5. Different particle need to be analyzed differently since their velocities varies as a function of their mass.

After some crude calculations it was found that for most incident angles the Čerenkov light produces fewer than a single photo-electron. Although a more detailed calculation should be done, we conclude that the Čerenkov signal from the window is small and can be made smaller by simple manipulations. We believe that this effect is in no way a fundamental limitation of the present design. Future prototypes will be constructed so that a variety of incident angles can be experimentally tested.

## 7.9 Electronics

The signal generated by each pad is sent through a series of electronics before being read by an ADC. The chain consists of a preamplifier, a isolation transformer, a shaping amplifier, and a CAMAC wide gate ADC. The preamp is mounted to the back flange of the vessel. Signals are carried from the

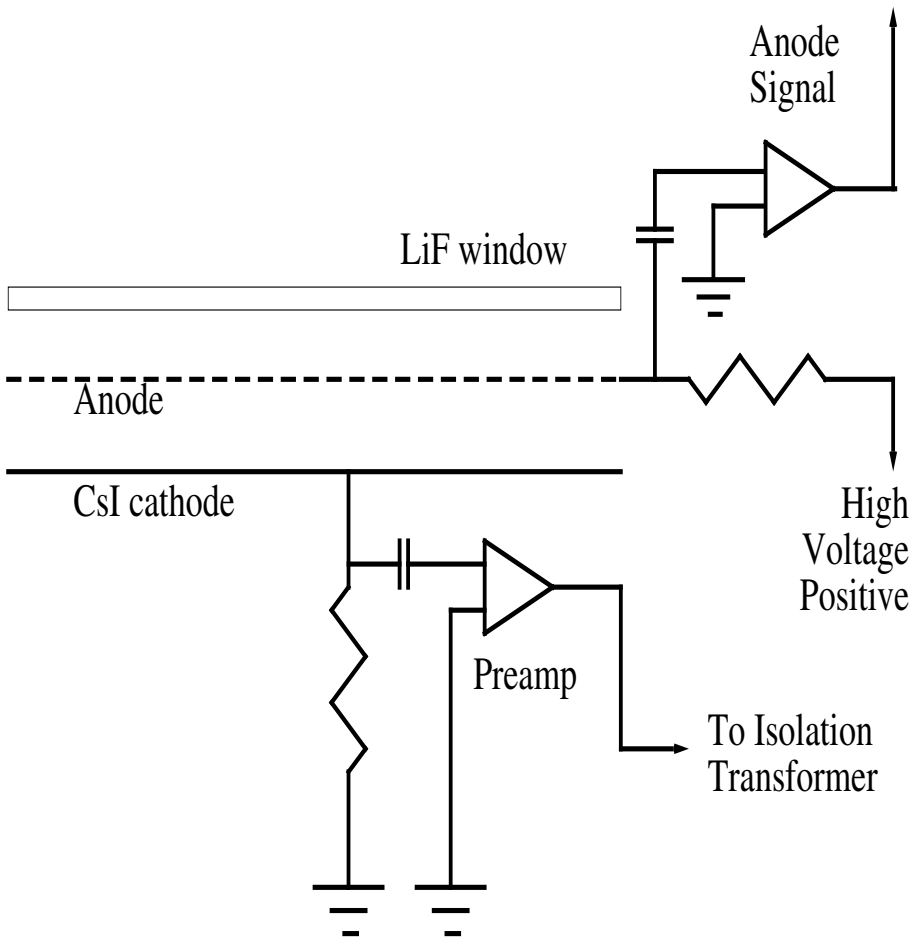


Figure 7.15: Schematic of HBD electronics. Note the additional circuit which digitizes the anode signal.

pad plane via Teflon insulated wires to the custom feedthroughs. From the feedthroughs the signal is taken to the preamp card with shielded 50 Ohm wired. Twist and flat cables connect the preamps to the isolation transformers which passively remove any DC offset from each AC coupled signal. From there, the signal is taken to the shaper with another set of twist and flat cables. After the shaper, the signal is sent to a wide gate ADC (LeCroy 2249W ADC). The data is collected with a 386 PC.

### 7.9.1 Preamplifier

The preamplifier used for the HBD is charge sensitive and converts the charge signal of the PPAC into an output voltage whose amplitude is proportional to the amount of input charge (0.5 V/pC). The preamplifiers used were designed at Brookhaven National Lab's Instrumentation Division by Stephani and are now manufactured by REL Labs in Hicksville, NY(model RL-789/3) Each chip is a hybrid triple pre-amp and contains three channels of very low noise preamplification (roughly 1000e's RMS).

### 7.9.2 Shapers

The shaping amplifiers used were designed and produced by Brookhaven National Lab's Instrumentation Division (model IO533). They are 200ns bipolar shapers that reduce the duration of the signal pulse arriving from the preamplifier. In doing this, it limits the bandwidth for the reduction of noise.

# Chapter 8

# Beam Tests

The HBD detector was tested at the Brookhaven National Laboratory's Alternating Gradient Synchrotron (AGS). The 29 GeV/c primary proton beam was incident upon a thick production target. The B2 test beam line views that target with double focusing momentum analyzing spectrometer. A Pb sheet was placed at the entrance of B2 to induce photon conversions and increase the fraction of electrons present in the beam.

## 8.1 Run History

In order to understand the results present, a brief discussion of the history of the run is necessary. The test run for the HBD occured in June 1994. The first days of the run were detected to tune-up of the data acquisition and the triggering system. During tune-up, UHP nitrogen was flowed (10 liters/mn)through the radiator. This was because $C_2F_6$ and $CF_4$ are very expensive ($2500 for 70lb cylinder). The nitrogen flow was also beneficial in

that it significantly reduced the detector's water and oxygen contamination.

The first radiator gas used was $CF_4$. On line analysis was not as expected. There were significantly fewer pads hit than there was expected. The Transparency Monitor reviewed that there was a loss of 33% in the transmission. It was later found that the bottle sent to us by MG industries was of a low purity. Tests of $CF_4$ were then aborted and $C_2F_6$ was then flowed as a radiator gas with a 1.2 meter length. The transparency recovered to about 90% at 156nm, but persistent contamination of the data set is probable.

The next two runs were done during times that Brant Johnson (B2 test beam Liaison Physicist for PHENIX) found "in the margins". An 80cm radiator length $C_2F_6$ data set was collected. We were only able to collect some data at this time because of AGS trouble. We also attempted to get 40cm radiator length data set. Even less data was collected at this length, because of an AGS vacuum leak. We were collecting 3 events per 3 second spill when normally sever hundred are expected. A few hours later, a neighboring experiment imploded, shutting of the beam entirely. Below is a listing of the run schedule.

1. $N_2$ with no Lead Glass
2. $N_2$ with Lead glass
3. $CF_4$ with Lead Glass
    (a) $CF_4$ found to be no good (99.0%)
    (b) Push out with $C_2F_6$ (unfortunately)

4. $C_2F_6$ with Lead Glass

5. Flow Nitrogen for a day

   (a) Order more $C_2F_6$ and get it in time

   (b) Request right purity of $CF_4$ but don't get it in time

6. Run $C_2F_6$ at 80cm (get some data)

7. Try to take data at 40cm (get very little data)

   (a) AGS vacuum leak, dump beam into C line

   (b) After begging at 3am, we get a little beam (3 to 4 events per spill)

   (c) Mid morning, neighboring experiment implodes (no more beam)

## 8.2 Trigger and Hit Definition

In order to identify particles coming from the AGS, additional beam-line particle identifiers were necessary. Just prior to the second analyzing magnet, the beam passed through scintillator paddles (S2) and a Čerenkov detector (C1). After the magnet, the beam passed through a second Čerenkov detector (C2) and another pair of scintillator paddles (S3). The beam passed directly through the HBD and was finally incident upon a 6 x 6 x 18 inch Pb-glass block (PBGL). A small scintillator (1x1 cm, S4) was placed before the PBGL counter to ensure that the incident beam particle landed near the center of the PBGL. An "all charged" or BEAM trigger was formed by the logical AND:

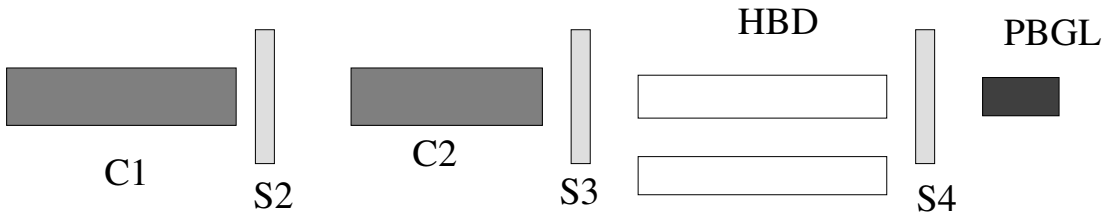


Figure 8.1: Configuration of the external triggers at the B2 test beam. Shown are 2 pairs of scintillation paddles (East and West), 2 Čerenkov detector, a finger counter (S4) and a Pb-glass block.

---

$BEAM = S2 \cdot S3 \cdot S4$. An electron trigger was formed by the definition: $ELECTRON = BEAM \cdot C1 \cdot C2 \cdot PBGL$. Although the ELECTRON trigger was used frequently in the early stages of the run for diagnostics, all data presented in this report were taken under the BEAM trigger. Shown in Figure 8.1 is the configuration of the external triggers at the B2 test beam.

Clean electrons were defined off-line by demanding a proper pulse height in each scintillator, firing of both Čerenkov counters, and full energy deposit in the Pb-glass counter. Clean pions were defined by demanding proper pulse height in each scintillator, pedestals in both Čerenkov detectors and "punch-through" in the PBGL counter. The HBD was **not used** in the event selection.

A cathode pad was defined as having been struck if that pad's pulse height was greater than 3.5 sigma above the pedestal. Pedestal runs were taken with the beam off. Figure 8.2 shows the configuration for both regular data taking and pedestal runs. Figure 8.3 shows histograms of some of the trigger signals collected over a run.

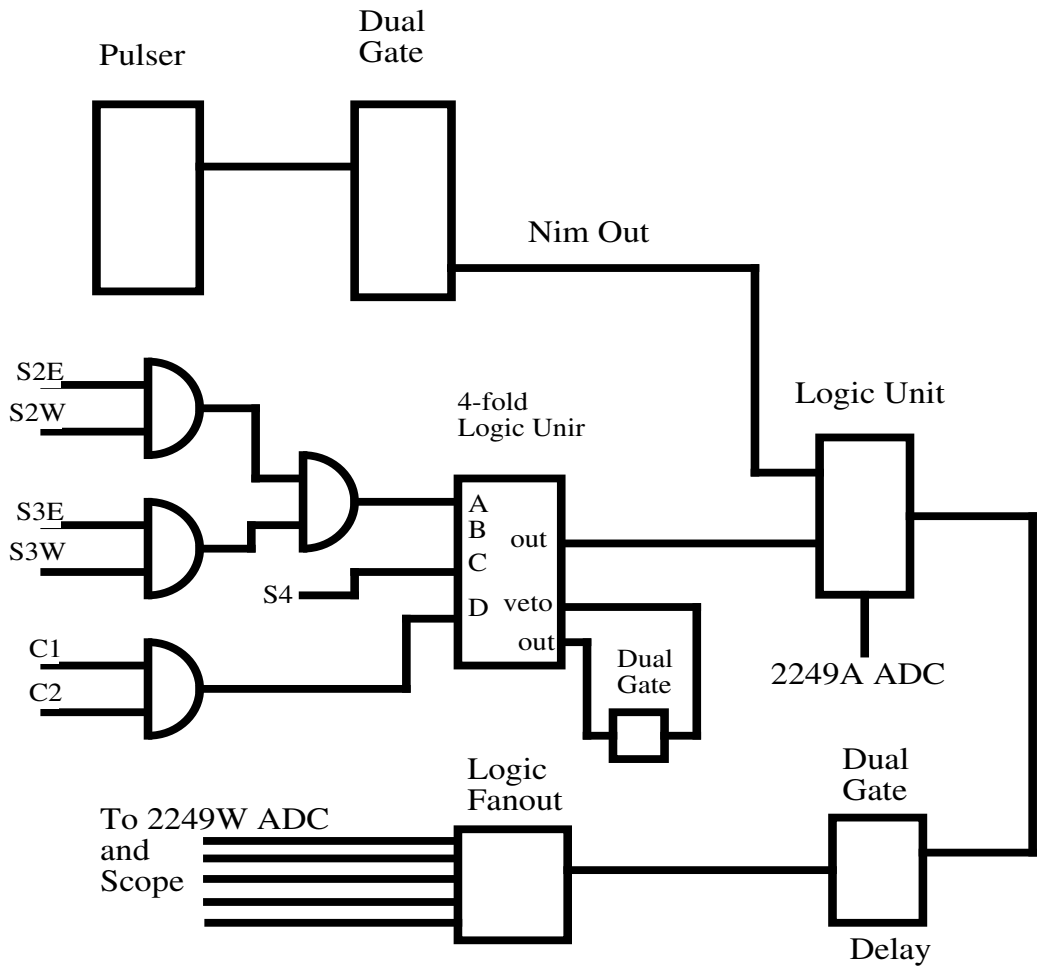


Figure 8.2: Triggers electronics at the B2 test beam.

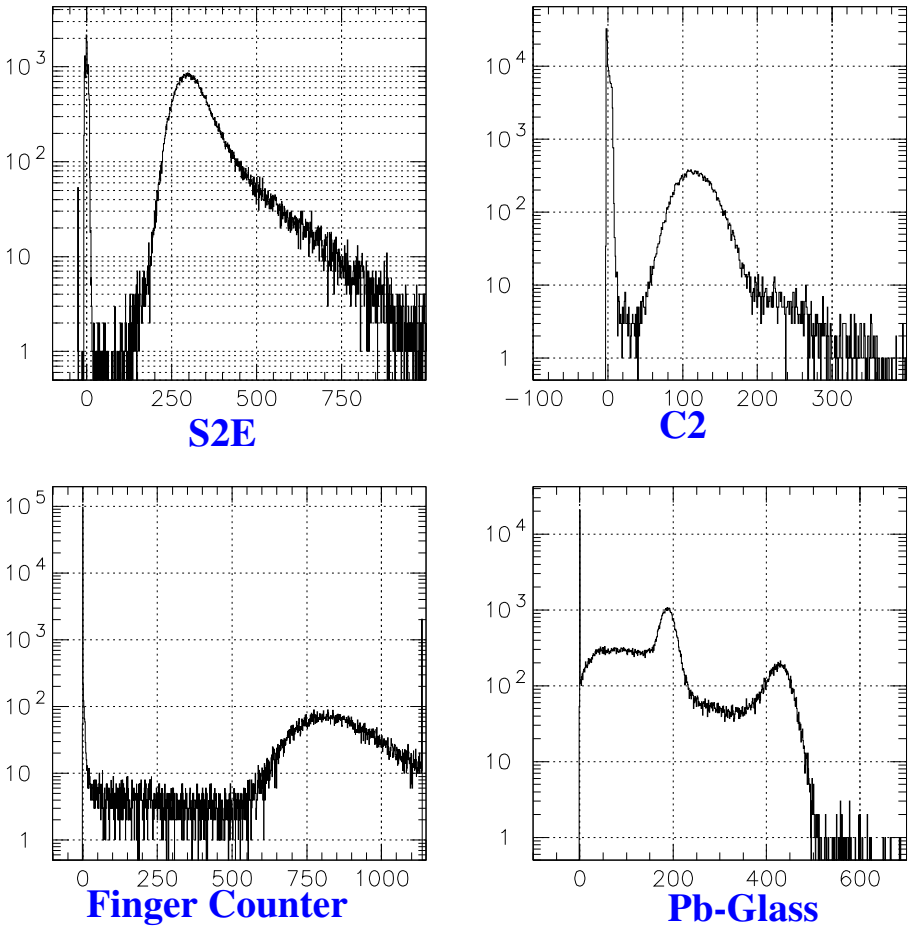


Figure 8.3: Plots of trigger signals. Shown is scintillation paddle 2 East, Čerenkov counter 2, the Finger counter and the Pg-Glass block. Note the pion punch through at 200 and the electron peak at 450 of the Pg-Glass block. (X-axis is ADC channel)

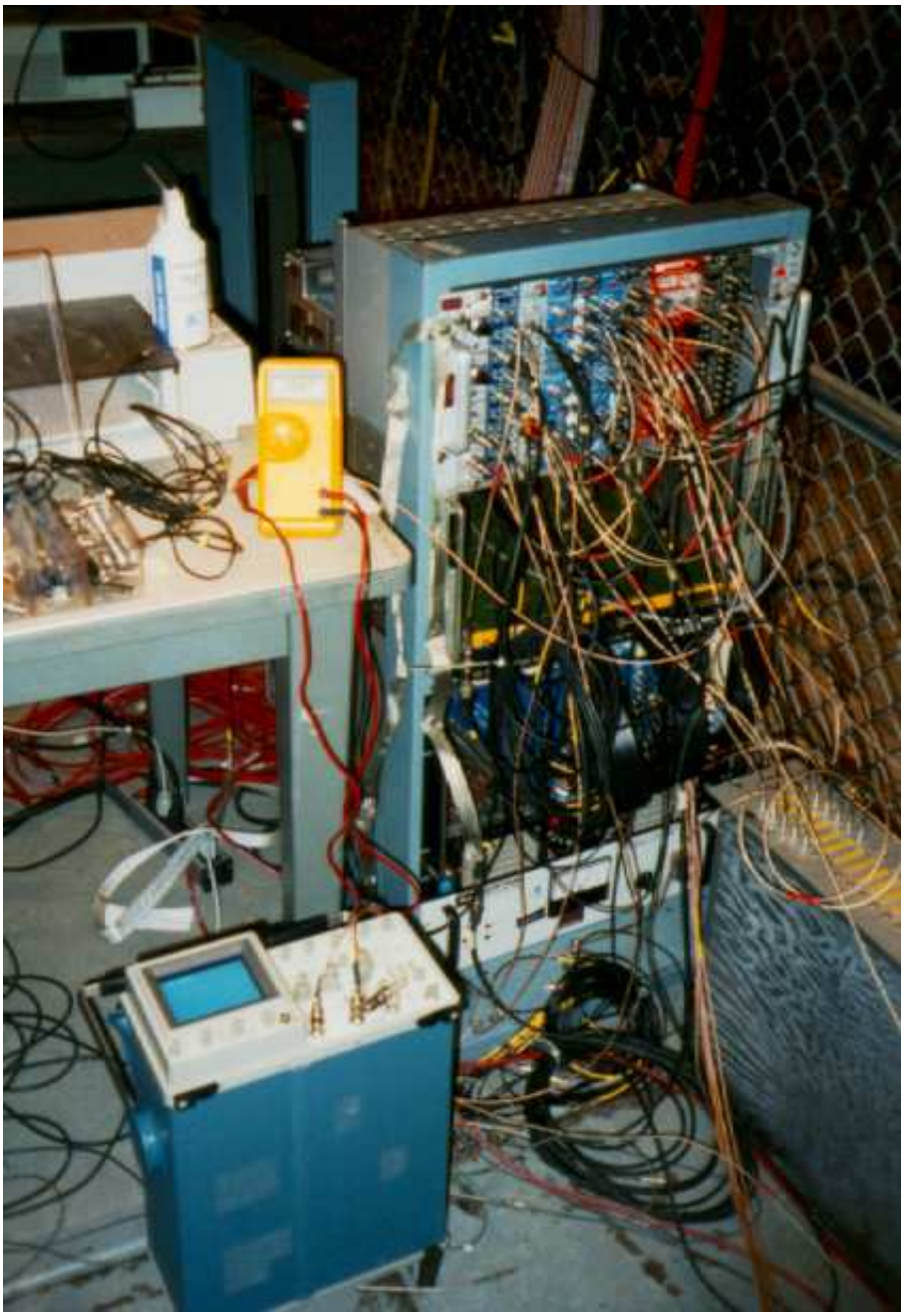

Figure 8.4: Photo of the electronics setup used for the test beam run.

## 8.3 Data Analysis

Three data sets were taken with the $C_2F_6$ radiator. The first used a radiator length of 1.2 meters, the second 80 cm, and the third 40 cm. Lengths were set by repositioning the light blocking sail. Unfortunately, just prior to the 1.2 meter length running a low purity (99.0%) bottle of $CF_4$ was run through the radiator vessel. The transparency monitor registered only 2/3 transmission at 156 nm while running this bottle. Although the transmission recovered to roughly 90% during the $C_2F_6$ run, it is suspected that some residual contamination may have reduced transmission and consequently detector performance at other wavelengths. Such possible contaminations were not present during the shorter radiator length tests.

### 8.3.1 The 120 Centimeter Length

Figure 8.8 shows the truly typical response of the detector to electrons. In this figure, we have plotted the very first 25 electron events in sequence from a $C_2F_6$ run at 120 cm length. Shaded pads are those defined as struck under the criteria listed above. Electrons clearly fire numerous pads on a single event. Figure 8.7 shows the detector's response to the very first 25 pion events in sequence from the same tape. Zero or one struck pad is the most likely response of the detector to the passage of a pion. These events are truly typical since even the run from which they were chosen was selected randomly.

The results in Figure 8.10 are accumulated over all available data at the

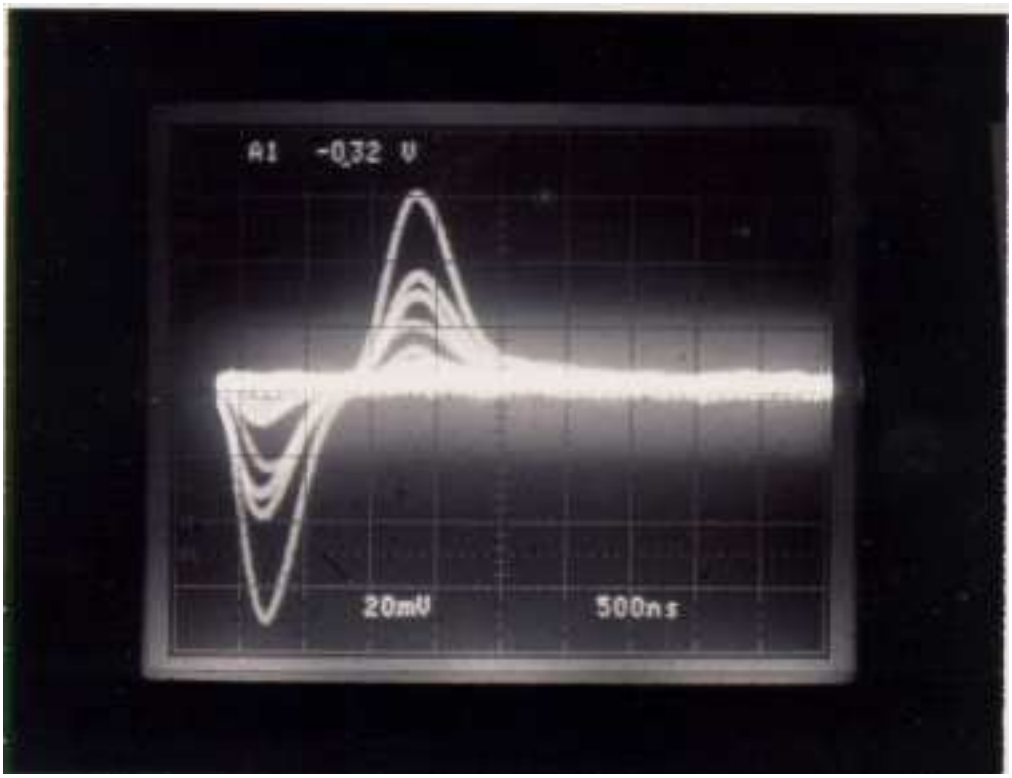


Figure 8.5: This is the signal from the anode just prior to Photo of the electronics setup used for the test beam run.

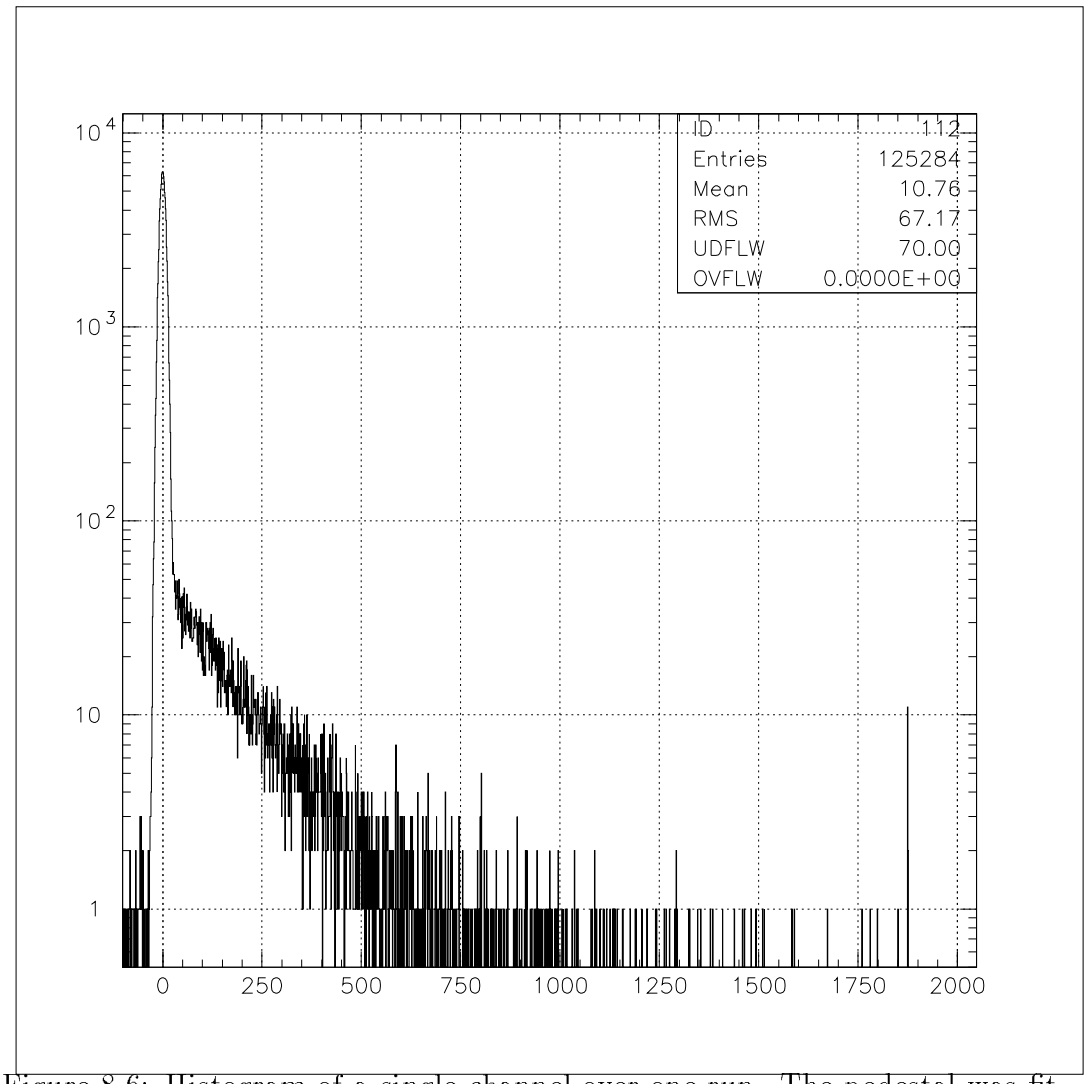


Figure 8.6: Histogram of a single channel over one run. The pedestal was fit to a Gaussian and a hit was defined as 3.5 sigma above pedestal.(X-axis is ADC channel)

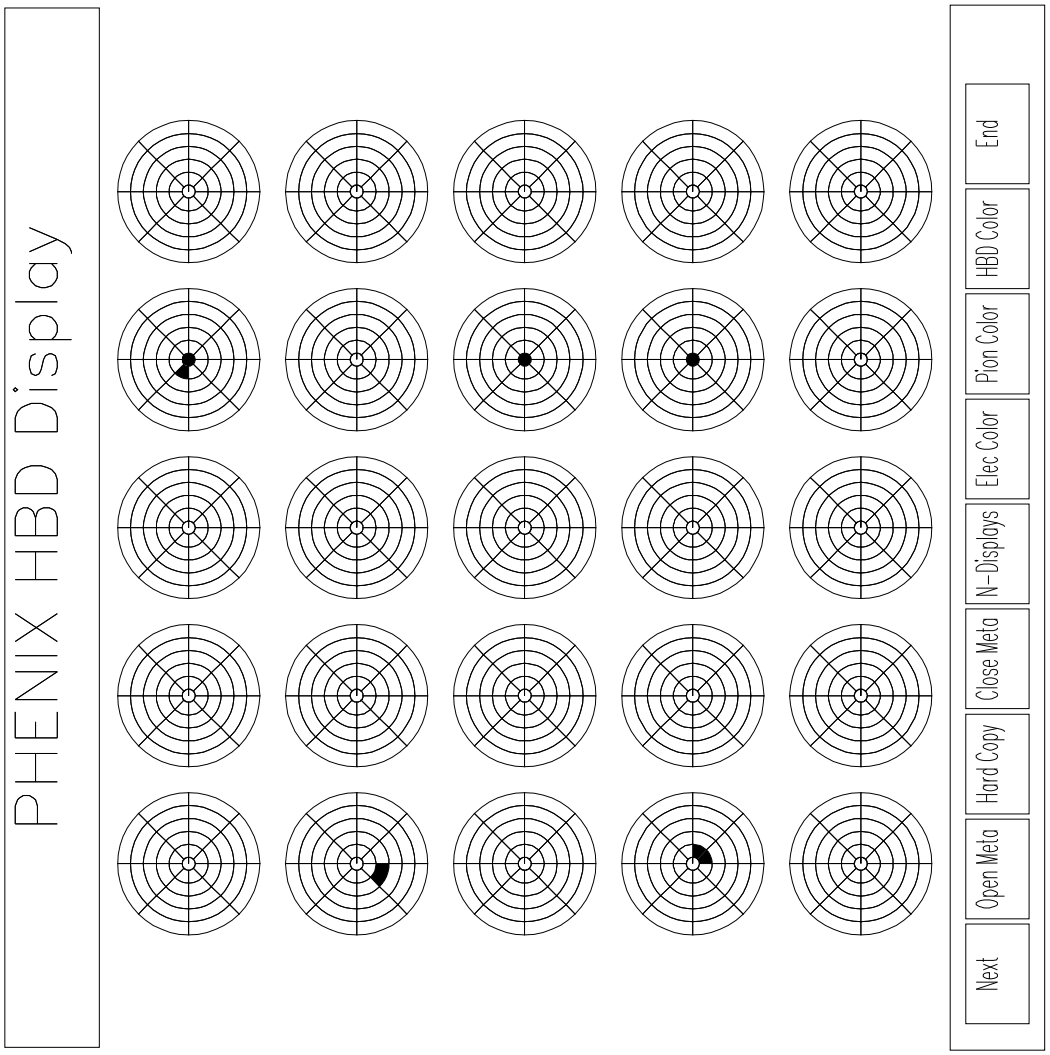


Figure 8.7: Shown here is the first 25 events defined as pion by external triggers. Mean number of pads is roughly .6.

Figure 8.8: Shown here is the first 25 events defined as electrons by external triggers. Mean number of pads is roughly 10.

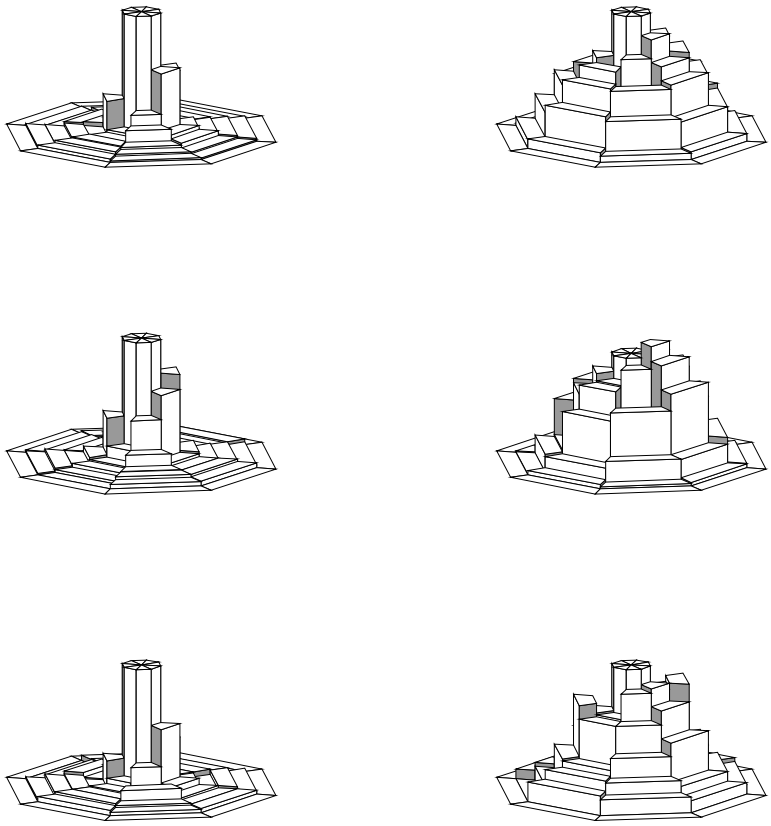

Figure 8.9: Figures show the mean number of pads hit over a collected run. On the left are pions and on the right electrons. From top to bottom is the 120cm, 80 cm and 40cm length.

120 cm radiator length. The top panel shows the probability of a given number of pads firing. Pions are represented by the solid line and electrons by the dashed line. The mean number of pads fired per pion is 0.6 with a most likely number of zero. Electrons fire a mean of ten pads. The bottom panel shows the spectrum of pulse heights measured by the digitization of the anode. Again, excellent separation of electrons and pions is apparent. These two variables (anode pulse height and number of pads) can be plotted in the form of a scatter plot as shown in top panel of Figure 8.11. Here the crosses represent the detector response to particles that the beam logic identified as electrons, and open circles represent the response to pions. The separation between pions and electrons is apparent. Two aspects of the detector response distinguish electrons from pions: total charge deposited and number of pads fired. It is instructive to analyze the rejection power of each of these measures independently. First, we consider the limit of an unsegmented or coarsely segmented detector in which the only possible separation technique is pulse height. Electrons would be chosen by requiring a total charge deposit above a certain threshold. Both the electron efficiency and the pion contamination will be a function of the cut threshold. The crosses in Figure 8.12 show the pion efficiency vs. the electron efficiency achieved by various cuts on anode pulse height. We can generate a series of such curves by additionally adding cuts on the minimum number of pads fired. These curves are also shown in Figure 8.12. The best chamber performance is achieved by a combination of both cuts. At 95% electron efficiency, the pion efficiency is 1/333. At 90% electron efficiency, the pion efficiency is 1/910.

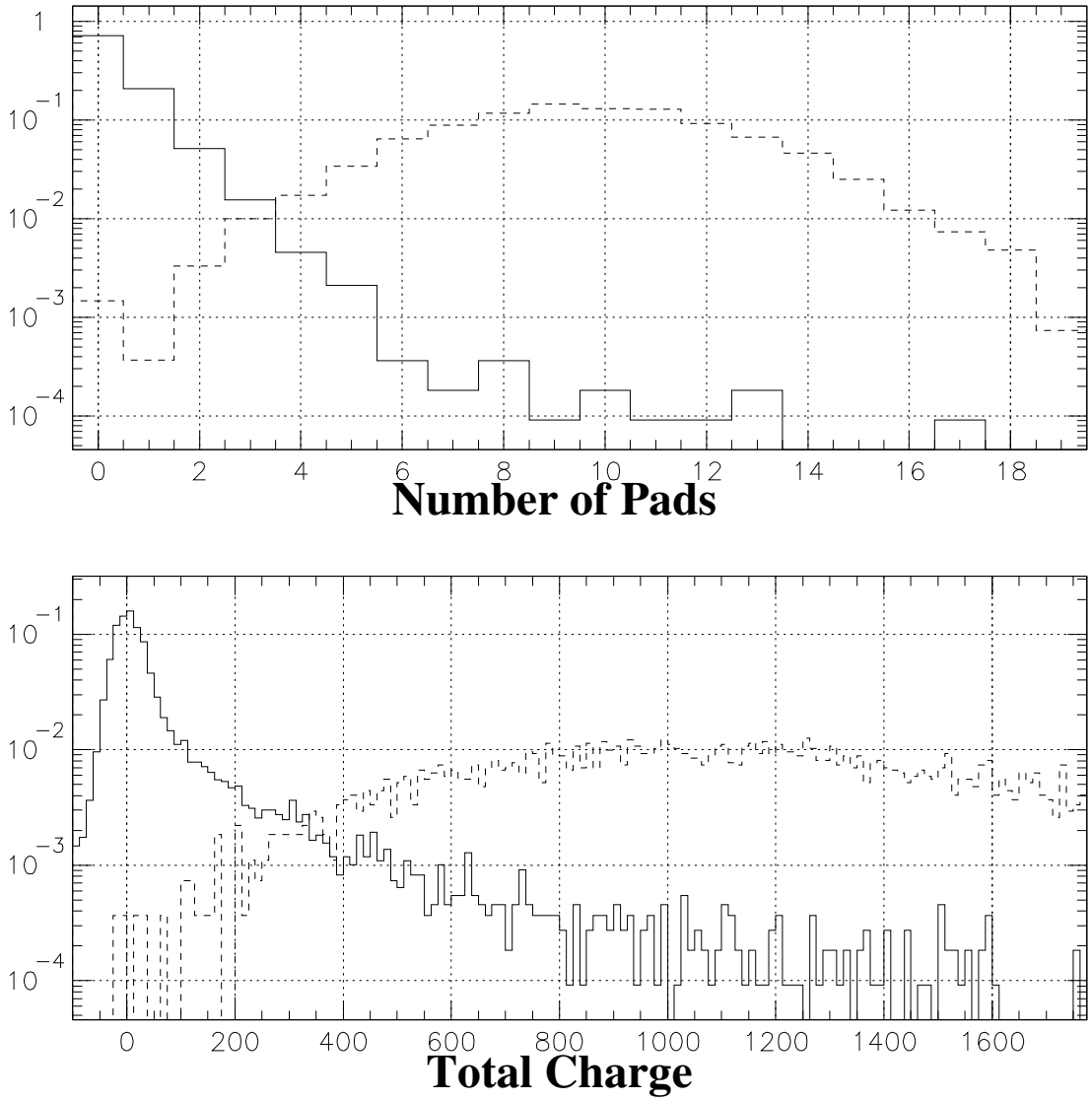


Figure 8.10: Upper Panel This figure shows the distribution of hit pads for electrons (dashed lines) and pions (solid lines) Lower Panel This figure displays the total charge collected on the cathode by an electron (dashed line) and a pion (solid line).

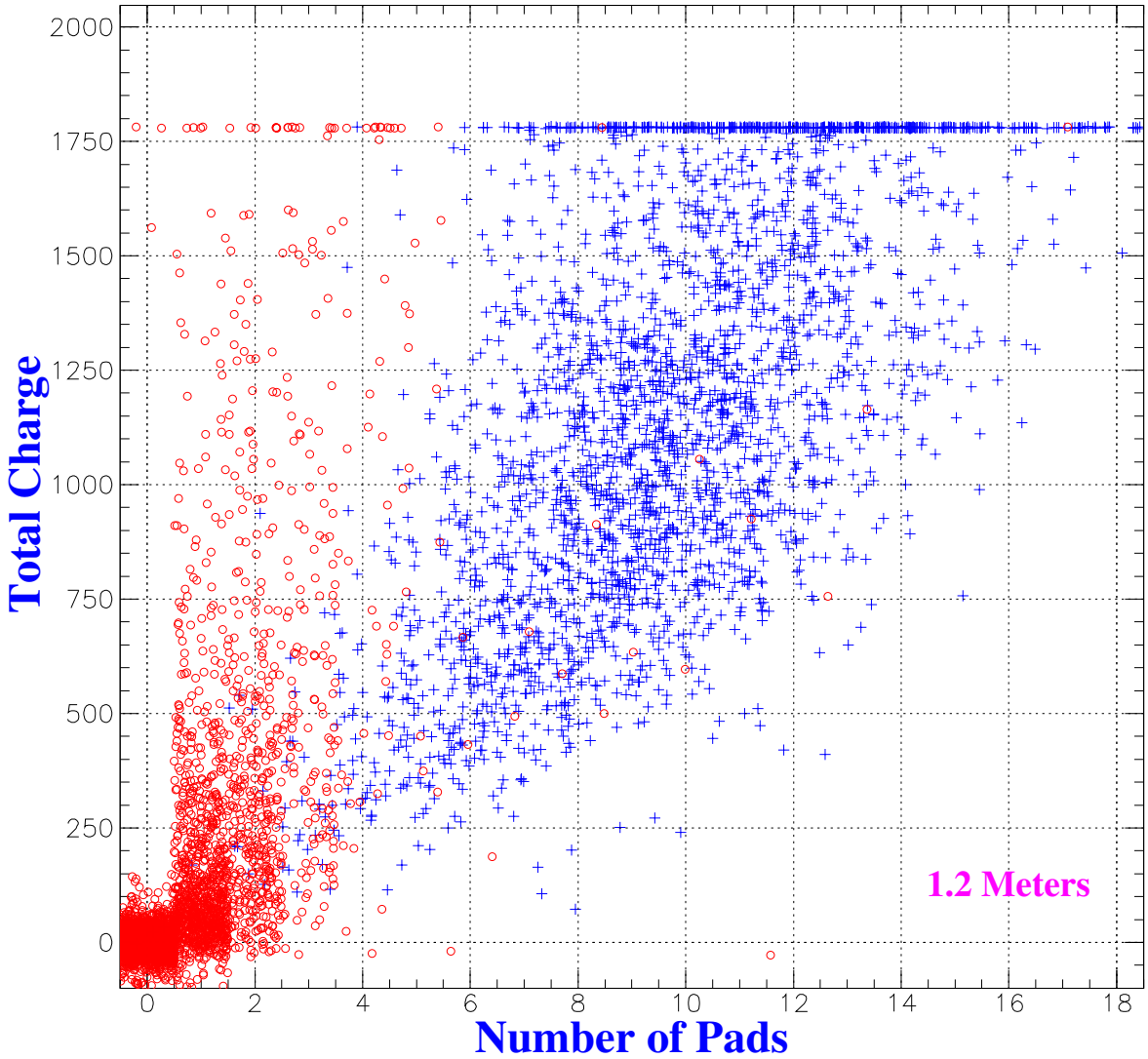


Figure 8.11: This is a graph of the total charge plotted verse the number of pads that fire. A clear separation between the pion (circles) and electrons 9 (crosses) can be seen.

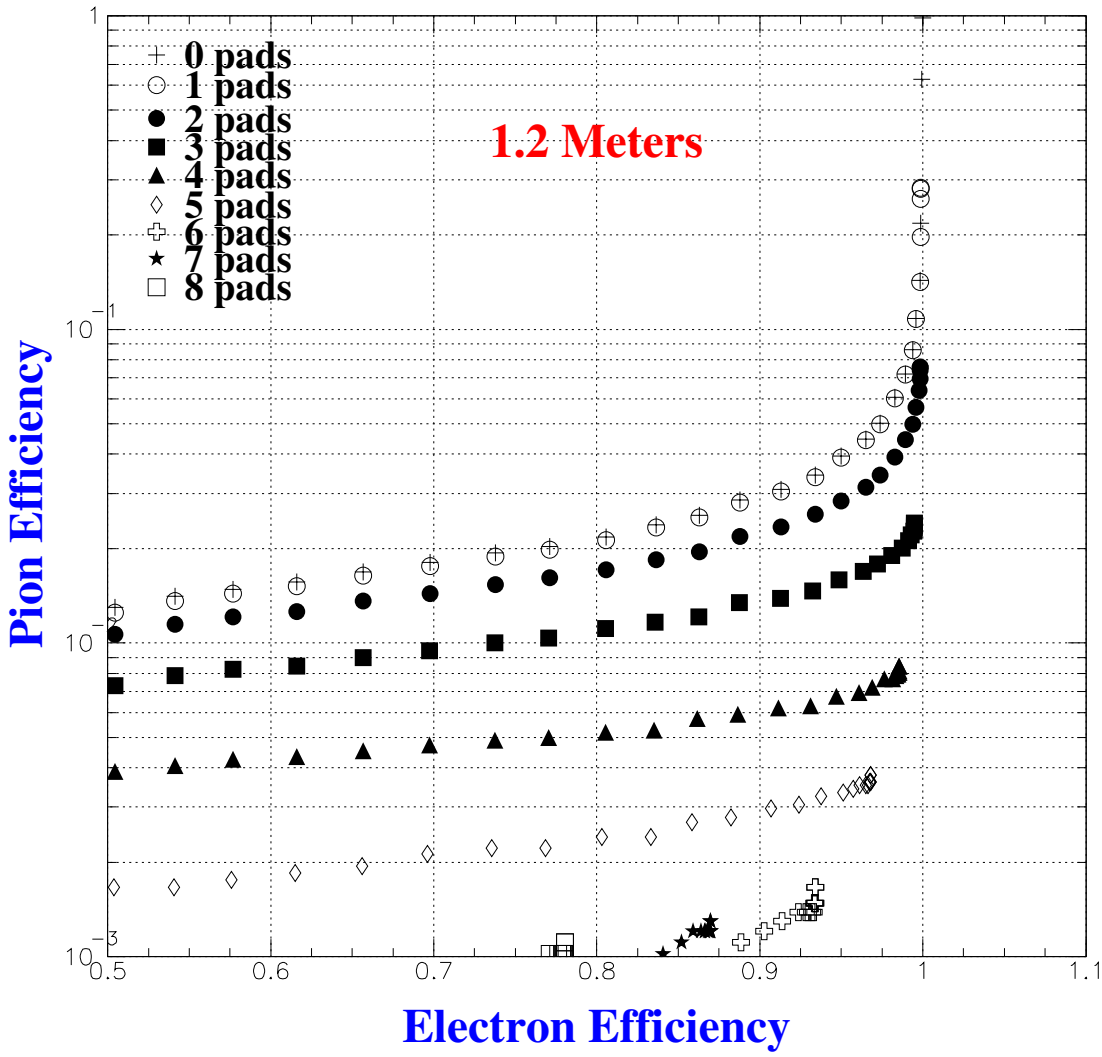


Figure 8.12: This plot shows the HBD's efficiency for Pions and Electrons at 120cm with $C_2F_6$ as a Radiator gas.

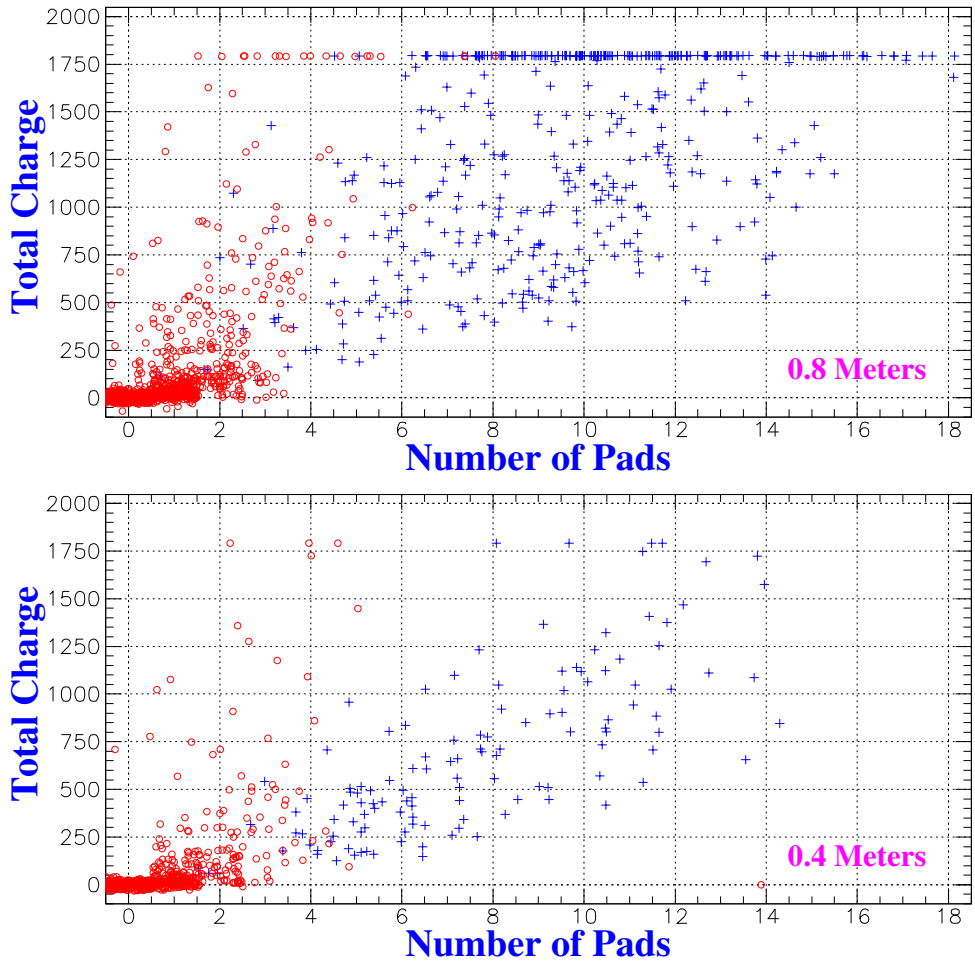


Figure 8.13: The upper panel shows the electron-pion separation for the 80 centimeter radiator length. The lower panel shows the separation of e/pi separation for the 40 centimeters length. Here, circles label pion and crosses label electrons.

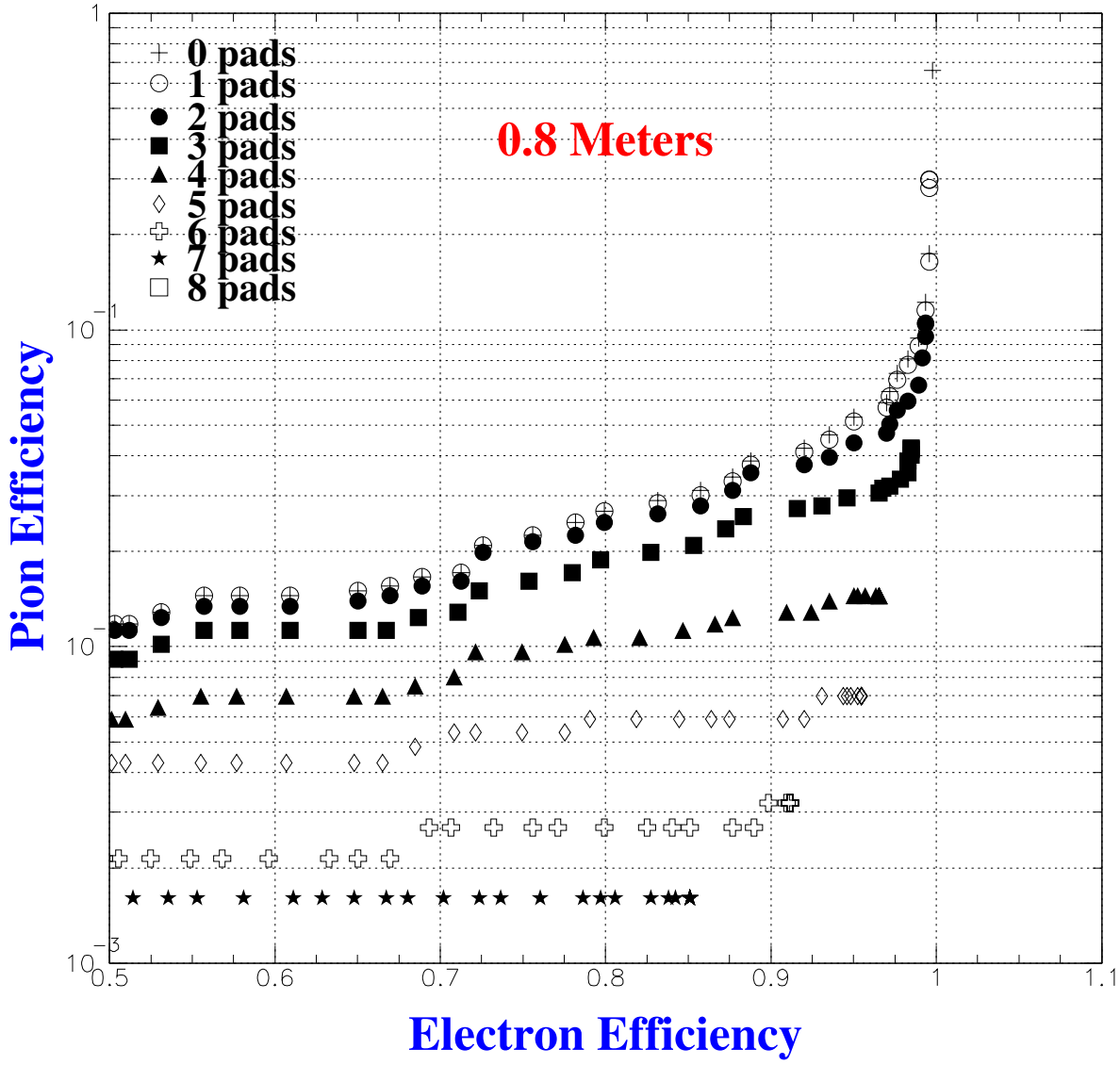


Figure 8.14: This plot shows the HBD's efficiency when operating with an 80 cm radiator.

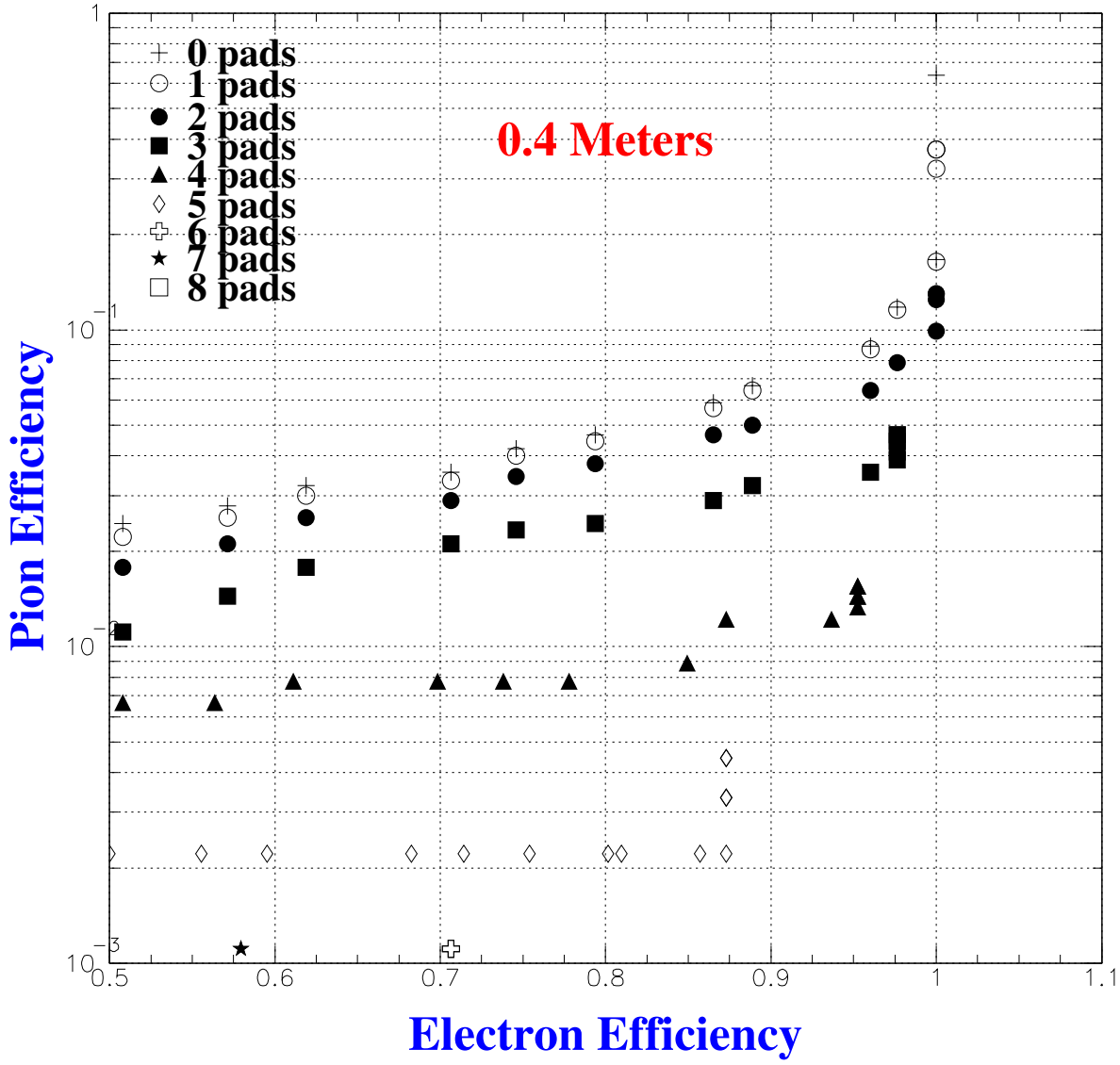


Figure 8.15: This plot shows the HBD's efficiency when operating with an 40cm radiator.

| **RadiatorLength** | $\epsilon_{\mathbf{electron}}$= **0.95** | $\epsilon_{\mathbf{electron}}$= **0.90** |
|---|---|---|
| 40 | 1/100 | 1/140 |
| 80 | 1/150 | 1/333 |
| 120 | 1/333 | 1/910 |

Table 8.1: This table shows the HBD's Pion efficiency for electron efficiency of 95% and 90%.

### 8.3.2 The 80 and 40 Centimeter Lengths

Also shown in this Figure 8.13 is the e/pi separation at the 80cm and 40cm runs. It should be noted that the statistics for the 80 and 40cm runs were much lower than that of the 120 cm run because of operating complications with the AGS during our test run. The total charge in these shorter lengths were also attenuated by a factor of two to keep them on scale.

Similar analysis can be performed on the data sets for the 80 cm and the 40 cm radiator lengths as mentioned for the 120 cm length. Figures 8.14 show the analysis performed on the 80 cm radiator length data. Figures 8.15 show the result for the 40 cm radiator length runs. Table 8.3.1 summarizes the results of pion rejection at the three lengths of radiator for both 95% and 90% electron efficiency.

Taking a factor of 100 rejection as the definition of hadron blind, we can declare our hadron blind detector to be successful at lengths as short as 40 cm.

# Chapter 9

# Conclusion

We have designed, constructed, and successfully tested the first working hadron blind detector. The detector varies from the original design of Giomataris and Charpak by the introduction of a crystal window (LiF) to separate the radiator and avalanche volumes. By choosing LiF (the lowest Z crystal in nature) we have added minimal thickness to the detector and maintained maximal transparency. The window allows for flexibility in the radiator gas choice, eliminating concerns about avalanche characteristics and chemical mischief in the presence of the CsI cathode. We have developed a stress eliminating fixture and gas flow topology (bubbling detector gas into the radiator) to protect the window against breakage. This HBD used a $C_2F_6$ radiator gas with a $He + 5\% CH_4$ as an avalanche mixture.

We have developed a thin yet high and uniform gain PPAC using the hexcell sandwich technique. The cathode plane has an embedded heater and thermocouple useful for warming the cathode during CsI deposition and vacuum baking. The PPAC assembles quickly (drop in parts, HV spring contacts,

slide-in gas fittings) and includes a self-aligning feature ensured by the grid spacer ring. The pad plane uses Ni and Au electroless plating to make it chemically compatible with the CsI overcoating. Custom multi-pin inexpensive, hermetic connectors were developed and have been adopted for use in the PHENIX RICH as well.

We have successfully produced high quality cathodes at Stony Brook using no extraordinary measures beyond cleanliness, good vacuum, and warming of the cathode during and after deposition. Presently nine cathodes have been made and are are of equal quality as those fabricated by the Particle Detector Group at FNAL.

We have tested the HBD in a beam of electrons and negative pions using a $C_2F_6$ radiator (high index of refraction, good transparency) and a helium (low $dE/dx$) methane avalanche gas mixture. Pion rejection was measured as a function of radiator length. Effective pion rejection at high electron efficiency has now been demonstrated in a compact, thin package (radiator lengths as short as 40 cm). At 95% electron efficiency, the pion efficiency was 1/333, 1/150, and 1/100 for 120, 80, and 40 cm. If 90% electron efficiency is used, the pion efficiency drops to 1/910, 1/333, and 1/140 for the above lengths.

The detector meets all criteria for a Phenix Dialtz rejector. Work done to present was performed as a test of concept and were very successful. Future goals would be to design and construct a large area LiF window and PPAC array for practical use in the Phenix detector.

# Bibliography

[1] Y. Giomataris and G. Charpak, Nucl. Instr. and Meth. A310 (1991) 589.

[2] D.F. Anderson, S. Kwan, and V. Peskov, Nucl. Instr. and Meth. A 343 (1994) 109.

[3] E. Aprile, A. Bolotnikov, D. Chen, et al,. Nucl. Instr. and Meth. A 343(1994) 129.

[4] C. Lu and K.T. McDonald Nucl. Instr. and Meth. A343 (1994) 135.

[5] C. Coluzza, J. Almeida, H. Berger, et al., Nucl. Instr. and Meth. A 343 (1994) 152.

[6] H. Brauning, A. Breskin, et al., Nucl. Instr. and Meth. A348 (1994) 223.

[7] B. Surrow, T. Hemmick, et al., Nucl. Instr. and Meth. A355 (1994) 342.

[8] A. Braem, A DiMauro, et al., Nucl. Instr. and Meth. A 343 (1994) 163.

[9] R. Aleksan, P. Besson, Ph. Bourgeois, et al., Nucl. Instr. and Meth. A343 (1994) 173.

[10] M. Staric, V. Cindro, S. Korpar, et al., Nucl. Instr. and Meth. A343 (1994) 192.

[11] J. Seguinot,G. Charpak, Y. Giomataris,et al., Nucl. Instr. and Meth. A297 (1990) 133.

[12] B. Hoeneisen, D Anderson, S Kwan, Nucl. Instr. and Meth. A302 (1991) 447

[13] V. Dangendorf, A. Breskin, R. Chechik, et el., Nucl. Instr. and Meth. A308 (1991) 519.

[14] D.F. Anderson, S. Kwan, V. Peskov, and B. Hoeneisen, Nucl. Instr. and Meth. A323 (1992) 626.

[15] R. Enomoto, T Sumiyoshi, and Y. Fujita, Nucl. Instr. and Meth. A 343 (1994) 117.

[16] G. Malamud, Ph Mine, D. Vartsky, et al., Nucl. Instr. and Meth. A348 (1994) 275.

[17] D.F. Anderson, S Kwan, and V. Peskov, Nucl. Instr. and Meth. A326 (1993) 611.

[18] J. Almeida, F. Barbo, M Bertolo, et al., Nucl. Instr. and Meth. A361 (1995) 245.

[19] A. Breskin, R. Chechik, et al., Nucl. Instr. and Meth. A 343 (1994) 159.

[20] Men Chen, Phenix Detector Councel Meeting, 1992.

[21] PHENIX Conceptual Design Report, Brookhave National Laboratory (1993).

[22] D.F. Anderson, S. Kwan, and V. Peskov, Nucl. Instr. and Meth. A348 (1994) 324.

[23] G. Malamud, P. Mine, et al., Nucl. Instr. and Meth. A 343 (1994) 121.

[24] W.R. Leo,*Techniques for Nuclear and Particle Physics Experiments*, Springer-Verlag, New York (1987)

[25] Donald Perkins, *Introduction to High Energy Physics*, Addison-Wesley Publishing Co., London (1982).

[26] B.R. Martin and G. Shaw,*Particle Physics*,John Wiley and Son, New York (1992).

[27] I.R. Kenyon, *Elenentary Particle Physics*, Routledge & Kegan Paul, New York (1987).

[28] I.S. Hughes, *Elementary Particles*, Cambridge University Press, New York (1991).

[29] Brend Surrow, *Prefromance of a Prototype Rich detector using a CsI Photocathode Readout*, Masters Thesis, SUNY Stony Brook (1993).

[30] R. A. Bersch, *Design, Implementation, and Results From a Position Sensitive Multiwire Proportional Chamber with Pad Readout*, Masters Thesis, SUNY Stony Brook (1993).

[31] Physical Review D, *Particles and Fields*, Volume 50 (1994) Number 3.

[32] W.Blum and L. Rolandi, *Particle Detection with Drift Chambers* , Springer-Verlag, New York (1993).

[33] Robert Sparrow, Optovac Corp., Acton Mass. Private Conversation

[34] H. Okabe and D.A. Becker, J. Chem. Phys. 39 (1963) 2549.

[35] B Guerard, P. Bruyndonckx, et al., Nucl. Instr. and Meth. A310 (1991) 116. Pion Rejection

[36] D.C. Imrie, A.H. Moghul, K. Wells, G. Charpak and V. Peskov, Nucl. Instr. and Meth. A310 (1991) 122.

[37] P. Fonte, V. Peskov, and F. Sauli, Nucl. Instr. and Meth. A310 (1991) 140.

[38] V. Peskov and A. Zichichi, Nucl. Instr. and Meth. A315 (1992) 77.

[39] Y. Giomataris, G Charpak, V. Peskov, and F. Sauli, Nucl. Instr. and Meth. A323 (1992) 431.

[40] H. Brauning, A breskin, et al,. Nucl. Instr. and Meth. A327 (1993) 369.

[41] P. Mine, Nucl. Instr. and Meth. A343 (1994) 99.

[42] A. Arefiev, G. Bencze, et al., Nucl. Instr. and Meth. A348 (1994) 318.

[43] A. Borovick-Romanov and V. Peskov, Nucl. Instr. and Meth. A348 (1994) 269.

[44] J. Almeida, H. Berger, A. Braem, et al., Nucl. Instr. and Meth. A348 (1994) 216.

[45] A. Pansky, A Breskin, R. Chechik, et al., Nucl. Instr. and Meth. A354 (1995) 262.

[46] V. Peskov, A. Borovick-Romanov, T. Sokolova, et al., Nucl. Instr. and Meth. A 353 (1994) 184.

[47] D.F. Anderson, R. Bouclier, G. Charpak, et al., Nucl. Instr. and Meth. 217 (1983) 217.

[48] W. Driscoll,*Handbook of Optics*, McGraw-Hill Book Co.,New York (1978).

[49] 1994 Oriel Cataloge

[50] Loren Morrow, ACE, private communication.